The Influence of an SST Front on a Heavy Rainfall Event over Coastal Taiwan during TiMREX

MICHAEL D. TOY* AND RICHARD H. JOHNSON

Department of Atmospheric Science, Colorado State University, Fort Collins, Colorado

(Manuscript received 25 October 2013, in final form 6 June 2014)

ABSTRACT

A long-lived heavy precipitation area was observed along the southwest coast of Taiwan from 13 to 18 June 2008 during the Terrain-Influenced Monsoon Rainfall Experiment (TiMREX). Rainfall amounts exceeded 500 mm along portions of the coast, and the coastal plains experienced severe flooding. The precipitation systems were influenced by blocking effects, as the southerly moist monsoon flow impinged on the island. A relatively strong gradient in the sea surface temperature (SST) off the southwest coast of Taiwan existed during the rainfall event. Mesoscale SST fronts are known to influence the planetary boundary layer (PBL) such that low-level convergence and precipitation are enhanced under certain circumstances. In this study, the authors investigate the role of the SST front in enhancing the 13–18 June 2008 precipitation event over Taiwan using the Weather Research and Forecasting (WRF) Model. In control simulations with the observed SST, there is a transition from a well-mixed to a stable PBL across the front, causing the low-level flow to decelerate, resulting in an enhancement of horizontal convergence. Such a transition in the PBL and the associated convergence is greatly reduced in smoothed SST gradient model simulations, which produce over 20% less precipitation over southwest Taiwan. Sensitivity tests show that, qualitatively, the results are independent of the existence of the island of Taiwan. These findings indicate that the SST gradient over the northern South China Sea during the early summer monsoon can have a significant impact on the intensity of rainfall over Taiwan.

1. Introduction

The yearly northward progression of the East Asian summer monsoon typically brings heavy rainfall to south China and Taiwan from mid-May to mid-June, a period known as the mei-yu season. The rainfall is mainly produced by mesoscale convective systems (MCSs) that propagate eastward along the subtropical mei-yu front and frequently bring more than 100 mm day^{-1} to the island of Taiwan (Ding and Chan 2005; Chen et al. 2007; Xu et al. 2009). The mei-yu frontal system is characterized by weak thermal contrast, a pronounced zone of cyclonic vorticity, and low-level convergence in association with a southwesterly low-level monsoon jet to the south of the front (Chen 1983). Particularly heavy rainfall events occur over Taiwan when the jet impinges on the island topography.

The influence on the synoptic-scale monsoon flow by the complex terrain of Taiwan has been the subject of much study (e.g., Kuo and Chen 1990; Chen 1992; Lin 1993; Li and Chen 1998; Yeh and Chen 2002; Wang and Chen 2003; Wang et al. 2005). The Central Mountain Range (CMR) runs along the island in a north–south direction with an average height of 2 km and peaks reaching almost 4 km. This isolated barrier locally enhances upwind precipitation amounts through orographic lifting and through induced offshore convergence due to blocking (Yu et al. 2001; Wang et al. 2005). Consequently, owing to the southwesterly monsoon flow, the highest frequency and largest amounts of rainfall during the mei-yu season occur over the southwest part of the island (Chen et al. 2007), a heavily populated coastal plain.

In the ocean waters off the southwest coast of Taiwan, a strong gradient in the sea surface temperature (SST) typically exists during the mei-yu period. The SST front

* Current affiliation: Institute for Mathematics Applied to Geosciences (IMAGe), Computational and Information Systems Laboratory, National Center for Atmospheric Research, Boulder, Colorado.

Corresponding author address: Dr. Michael D. Toy, National Center for Atmospheric Research, P.O. Box 3000, Boulder, CO 80307-3000.
E-mail: toy@ucar.edu

DOI: 10.1175/JAS-D-13-0338.1

sets up in the northern South China Sea (SCS) to the southwest and west of Taiwan during boreal winter (Chu and Chang 1997; Chu et al. 1997; Chen et al. 2003) and is associated with an extensive cold tongue that develops across the SCS (Varikoden et al. 2010). It results from the cold continental flow of the East Asian winter monsoon, which cools the waters to zonally anomalous low temperatures (Boyle and Chen 1987). The strong SST front typically disappears by July owing to the warm-air advection of the southerly summer monsoon. Johnson and Ciesielski (2002) speculated that the observed position of the primary rainfall maximum during the onset of the 1998 summer monsoon may have been related to the SST gradient through a modification of the planetary boundary layer (PBL) as the warm, moist southwesterly near-surface flow overruns the colder SSTs downwind of the front. The purpose of this paper is to explore the possibility that PBL flow modification by the SST front enhances the coastal and offshore monsoon rainfall over and near southwest Taiwan.

The Southwest Monsoon Experiment (SoWMEX) and the Terrain-Influenced Mesoscale Rainfall Experiment (TiMREX) were carried out jointly from May to June 2008 to study the causes of heavy rainfall events on the southern part of Taiwan associated with southwesterly monsoon flows (Jou et al. 2011). A number of heavy rainfall episodes were recorded during the experiments (Davis and Lee 2012; Xu et al. 2012; Ruppert et al. 2013). A particularly heavy rainfall period occurred during 13–18 June 2008 when two MCSs dropped over 320 mm of rain over coastal areas of southwestern Taiwan and caused major flooding. Davis and Lee (2012) and Xu et al. (2012) examine mechanisms, based on TiMREX data, for the enhancement of the coastal rainfall in relation to coastal fronts formed by convective cold pools blocked by the topography of Taiwan. In this paper we present a numerical model study of the 13–18 June 2008 event that reproduces the observed rainfall patterns. Sensitivity experiments to the underlying SST are performed to determine the influence of the SST front on the rainfall.

The effect of mesoscale SST fronts on boundary layer flow and precipitation has been studied extensively in the past decade as spaceborne measurements of SST, surface winds, and precipitation from platforms such as the Quick Scatterometer (QuikSCAT) and the Tropical Rainfall Measuring Mission (TRMM) have become available. Small et al. (2008) and Chelton and Xie (2010) provide reviews of research into this effect that reveals a strong interaction between SST fronts and near-surface winds in varied locations throughout the world, such as the Kuroshio, the Gulf Stream, and the Agulhas Current.

Lindzen and Nigam (1987) presented one of the first studies of the effect of large-scale SST gradients in the tropics on low-level winds, in which the air is assumed to remain in equilibrium with the surface. They found that observed anomalous winds associated with SST fronts could be explained by horizontal hydrostatic pressure gradients induced by variations in the temperature of the PBL. The anomalous surface winds flow down the pressure gradient from cool SST to warm SST near the equator, with the strongest winds in the SST frontal zone. Wallace et al. (1989) and Hayes et al. (1989) considered nonequilibrium flow over sharp SST gradients at oceanic mesoscales (~10–100 km) to explain surface wind variability over the eastern equatorial Pacific cold tongue. They argued that, in the case of flow from cold to warm SSTs, enhancement of surface fluxes causes a deepening of the PBL and mixing of high-momentum air aloft down to the surface. The result is that there is a positive correlation between wind speed and SST; namely, winds are stronger (weaker) over higher (lower) SSTs. Consequently, flow from warm to cool (cool to warm) SST will lead to surface convergence (divergence). In recent studies, it has been shown that modifications of PBL flow by mesoscale SST gradients can enhance low-level lifting and can trigger or enhance convective precipitation (Minobe et al. 2008; Xu et al. 2011; Li and Carbone 2012; Miyama et al. 2012), thus having an impact on atmospheric variability and climate.

During the TiMREX period, the SST front upwind of Taiwan was anomalously sharp compared to climatology according to SST observation products. The waters to the southwest of the island were warmer than average, and the waters to the west in Taiwan Strait were anomalously cold. In this paper, we use the Weather Research and Forecasting (WRF) Model (Skamarock and Klemp 2008; Skamarock et al. 2008) to analyze the effect of the SST front in the SCS on the 13–18 June 2008 rainfall events through ensemble simulations at a convection-permitting horizontal resolution. To draw out the influence of the SST front, we performed simulations with both the observed SST pattern and a pattern with a smoothed temperature gradient. While the previous studies of air–sea interactions along SST fronts have considered long-term climatic effects, we show that these interactions can have effects over a period of days and can affect the evolution of individual MCSs as observed during TiMREX. The data obtained during TiMREX are described in section 2. A description of the rainfall event is provided in section 3. Section 4 provides an overview of the observed SST pattern in the vicinity of Taiwan. In section 5 we present model simulations, which include a control run, reproducing the general characteristics of the observed heavy rainfall event, and sensitivity runs to determine the influence of the SST pattern and the topography of Taiwan on the rainfall event. A summary and conclusions are provided in section 6.

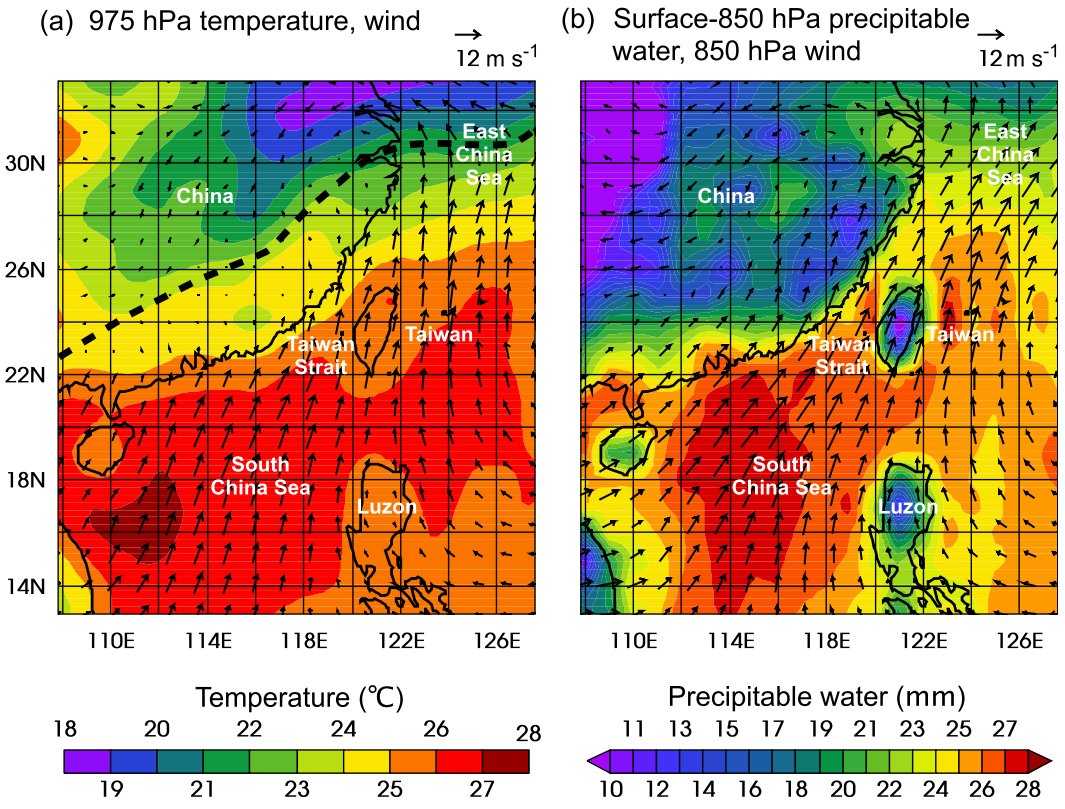

FIG. 1. Time-mean NCEP FNL Operational Global Analysis data for 0000 UTC 13 Jun–0000 UTC 18 Jun 2008: (a) 975-hPa temperature, wind, and position of mei-yu front (thick dashed line) and (b) surface–850-hPa-layer precipitable water and 850-hPa wind.

2. Data

The SST data we used for the lower-boundary forcing in the WRF Model runs are the daily real-time global SST (RTG SST) (Thiébaux et al. 2003) analyses of the National Centers for Environmental Prediction (NCEP) on a 0.5° grid. For the initial atmospheric conditions and forcing at the lateral boundaries, we used the 6-hourly NCEP FNL (Final) Operational Global Analysis data on a 1.0° grid, containing data at the surface and 26 pressure levels from 1000 to 10 hPa.

We present TiMREX data to provide an overview of the rainfall events and to compare with the model simulation results. Rawinsonde data from two locations that straddle the SST gradient to the southwest of Taiwan are used to demonstrate the effect on the PBL structure by the front. Soundings from the northern site on the island of Makung were measured with Vaisala RS80 sondes launched every 6 h, except during the intensive observing period 8 (IOP8) (14–16 June), when sondes were launched every 3 h. Soundings from the southern site were taken from a research ship with the Graw DFM-97 system launched from variable locations every 6 h. The sonde data underwent quality-control corrections to account for a dry bias found at some of the sounding sites and to correct for contamination of thermodynamic variables near the surface by the ship itself (Ciesielski et al. 2010).

The TRMM Multisatellite Precipitation Analysis (TMPA) 3B42 rain product (Huffman et al. 2007) at 0.25° × 0.25° resolution is used for visualizing the monsoon rainbands that were active over the region. For the localized rainfall in the Taiwan vicinity, we refer to the Quantitative Precipitation Estimation and Segregation Using Multiple Sensors (QPE SUMS) (Gourley et al. 2001) gauge-corrected radar-derived precipitation data provided by the Central Weather Bureau of Taiwan.

3. Overview of the 13–18 June 2008 rainfall events

There were two significant periods of heavy rainfall over southwestern Taiwan in June 2008 during TiMREX (Davis and Lee 2012). The first period (1–6 June) was characterized by MCSs and a mesoscale convective vortex (Lai et al. 2011), which developed over southern China and propagated eastward along the mei-yu front, located at that time in an east–west orientation along the southern edge of Taiwan. During the next heavy rainfall period (13–18 June) the mei-yu front had moved to the north of the island (Fig. 1a), and a southwesterly low-level

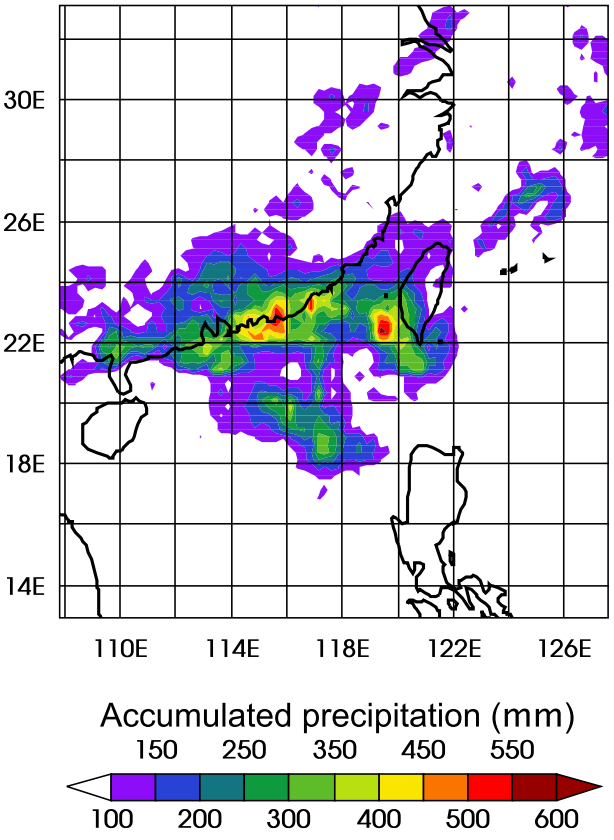

FIG. 2. TRMM 3B42 rainfall for 0000 UTC 13 Jun–0000 UTC 18 Jun.

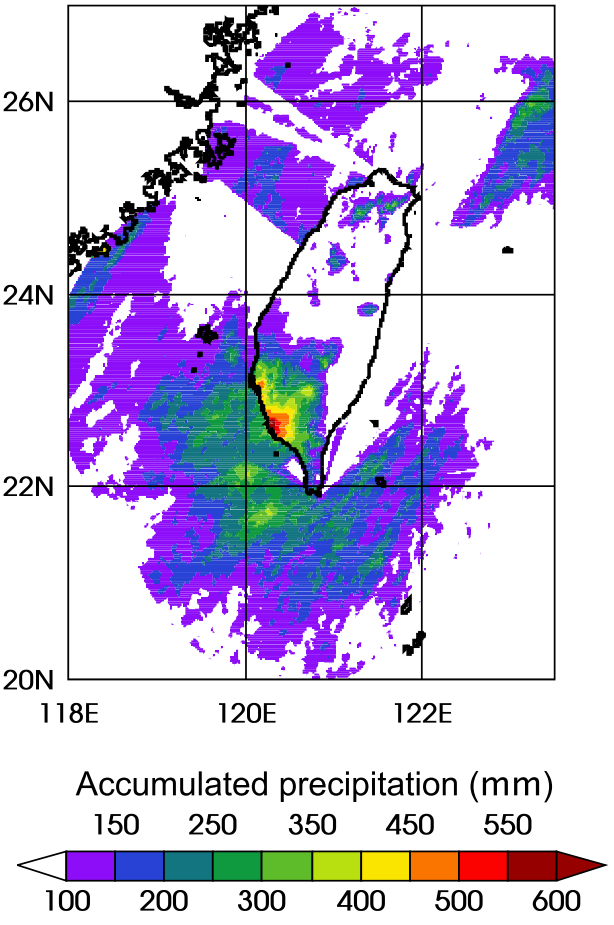

FIG. 3. QPE SUMS rainfall in the vicinity of Taiwan for 0000 UTC 13 Jun–0000 UTC 18 Jun.

jet (LLJ) persisted, causing warm, moist air to impinge on the island (Figs. 1a,b).

Figure 2 shows the TRMM 3B42 accumulated rainfall for the period 13–18 June over southeastern China, Taiwan, and the South China Sea. An east–west-oriented rain maximum is evident over Taiwan Strait extending to the south coast of China. During this 5-day period, heavy precipitation associated with a squall line fell on the southeast coast of China on 13 June and propagated southeastward toward Taiwan (Xu et al. 2012). On 16 June, a second disturbance developed just off the coast of southwestern Taiwan and moved onshore (Xu et al. 2012). Figure 3 shows the QPE SUMS rain gauge-corrected radar-derived rainfall estimates in the vicinity of Taiwan for the same period. The northern and eastern portions of the island received little precipitation compared to the southwest coastal plain, which had 5-day rainfall amounts exceeding 500 mm along portions of the coast.

The QPE SUMS data (Fig. 3) indicate that the maximum rainfall occurred inland, while the TRMM data (Fig. 2) show the maximum situated about 75 km off the southwestern coast and that precipitation amounts along the coast only reached 300–350 mm. We believe that QPE SUMS more accurately represents the inland rainfall amounts, as they were checked against rain gauge data (not shown). The TRMM 3B42 product uses merged infrared satellite observations of outgoing longwave radiation (OLR), which may account for the displacement of the rainfall maximum to the southwest. Xie et al. (2006) point out that use of OLR to infer convective precipitation confined to small regions is subject to errors due to the downwind displacement of convective anvils. This could be the case with the TRMM rainfall, as the tropopause winds were northeasterly during this period. On the other hand, there is a discontinuity in the QPE SUMS rainfall maximum along the southwestern coastline (Fig. 3), which, as pointed out by Davis and Lee (2012), is likely an artifact of there being no correction to the radar-derived rainfall applied over water. The radar may tend to underestimate the offshore rainfall because of possible calibration issues and because the lowest-elevation scan rapidly ascends above cloud-base level with increasing distance offshore.

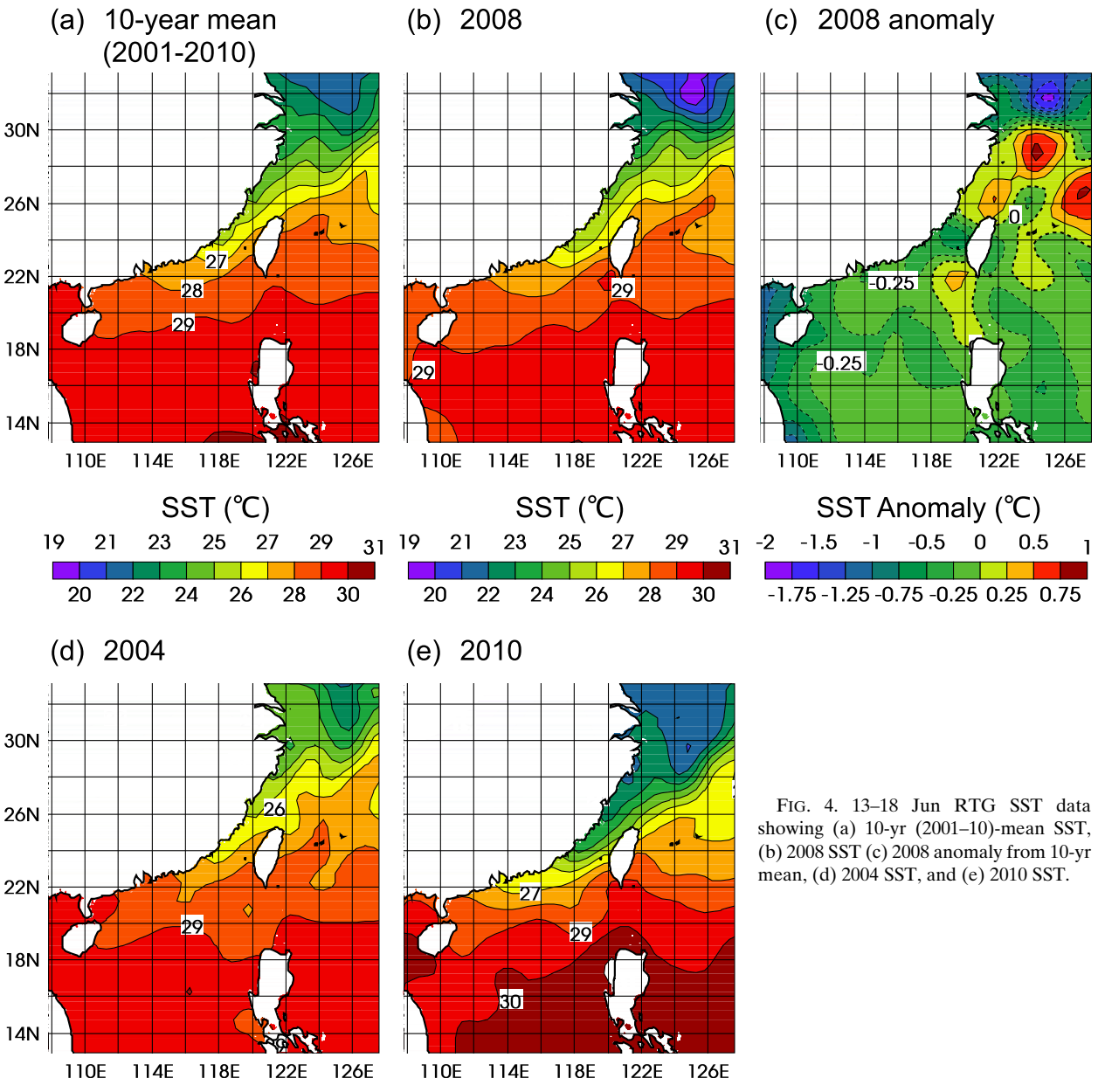

FIG. 4. 13–18 Jun RTG SST data showing (a) 10-yr (2001–10)-mean SST, (b) 2008 SST (c) 2008 anomaly from 10-yr mean, (d) 2004 SST, and (e) 2010 SST.

It is likely that the maximum rainfall occurred offshore, but at what distance from shore is not certain.

4. Sea surface temperature

The heavy rainfall that hit Taiwan during TiMREX was associated with MCSs that propagated over the South China Sea. It is therefore likely that the ocean had a large impact on these systems through surface latent heat, sensible heat, and momentum fluxes. The goal of this paper is to study this impact, particularly in relation to the SST front that is observed near Taiwan during the mei-yu period of the summer monsoon. Here, we briefly describe the climatology of SST patterns in the vicinity and describe the conditions present during TiMREX.

In late spring and early summer there is a remnant cold tongue in the northern South China Sea that forms during the East Asian winter monsoon (Chu and Chang 1997; Chu et al. 1997; Chen et al. 2003; Varikoden et al. 2010). The mean 13–18 June SST for the period 2001–10, based on RTG SST data, is shown in Fig. 4a. The SST south of Taiwan is warm and relatively uniform at about 29°–30°C. In Taiwan Strait to the west of the island, the temperature is much cooler and the southwest–northeast-oriented SST front is evident. During the period 13–18 June 2008, the SST gradient was stronger than average

(Fig. 4b), especially to the southwest of Taiwan. The temperature anomaly relative to the 10-yr mean (Fig. 4c) indicates that waters were anomalously warm (>0.25°C) off the southwest coast of the island and anomalously cool (<−0.5°C) to the north, which confirms the sharper SST gradient that existed during this time. During the 10-yr period (2001–10), the frequency of occurrence of strong, average, and weak mean 13–18 June SST gradients in Taiwan Strait were about evenly distributed. Figure 4d shows the SST pattern for 2004, a year with a weaker-than-normal SST gradient, and Fig. 4e shows the SST pattern for 2010, a year with a stronger-than-normal SST gradient. While we show only the 13–18 June means for 2004 and 2010, the strength of the SST gradient during this period is consistent with the seasonal pattern for each year. That is, the SST pattern generally persists within the time scale of the mei-yu season.

5. Model simulations

We performed model simulations to examine the effect of the sharp SST front in the northern SCS southwest of Taiwan on the intensity of the rainfall events of 13–18 June 2008. As is observed with mesoscale SST fronts in other parts of the world (Small et al. 2008; Chelton and Xie 2010), we are looking for enhanced low-level convergence over the front associated with a transition from a well-mixed to stable planetary boundary layer as the warm southerly surface winds overrun the colder waters to the north. Given sufficient moisture and instability, the low-level convergence would enhance convection through rising motion. Sensitivity experiments with a smoothed SST front were performed to see if the low-level convergence and associated rainfall are reduced.

For our experiments, we used the WRF Model configured with the Advanced Research WRF (ARW) dynamical solver. We used a convection-permitting horizontal grid spacing of 3 km with 610 × 432 grid points in the zonal and meridional directions, respectively. The horizontal model domain is shown in Fig. 5. In the vertical, we used a stretched grid with 60 levels, and the model top was set to 50 hPa. The microphysics scheme is the WRF single-moment 6-class scheme (Hong and Lim 2006), and the boundary layer scheme is the Yonsei University (YSU) (Hong et al. 2006) scheme. The shortwave radiation scheme is the Dudhia scheme (Dudhia 1989), and for longwave radiation we use the Rapid Radiative Transfer Model (RRTM) (Mlawer et al. 1997).

We performed four sensitivity experiments to determine the effects of the sea surface temperature, as

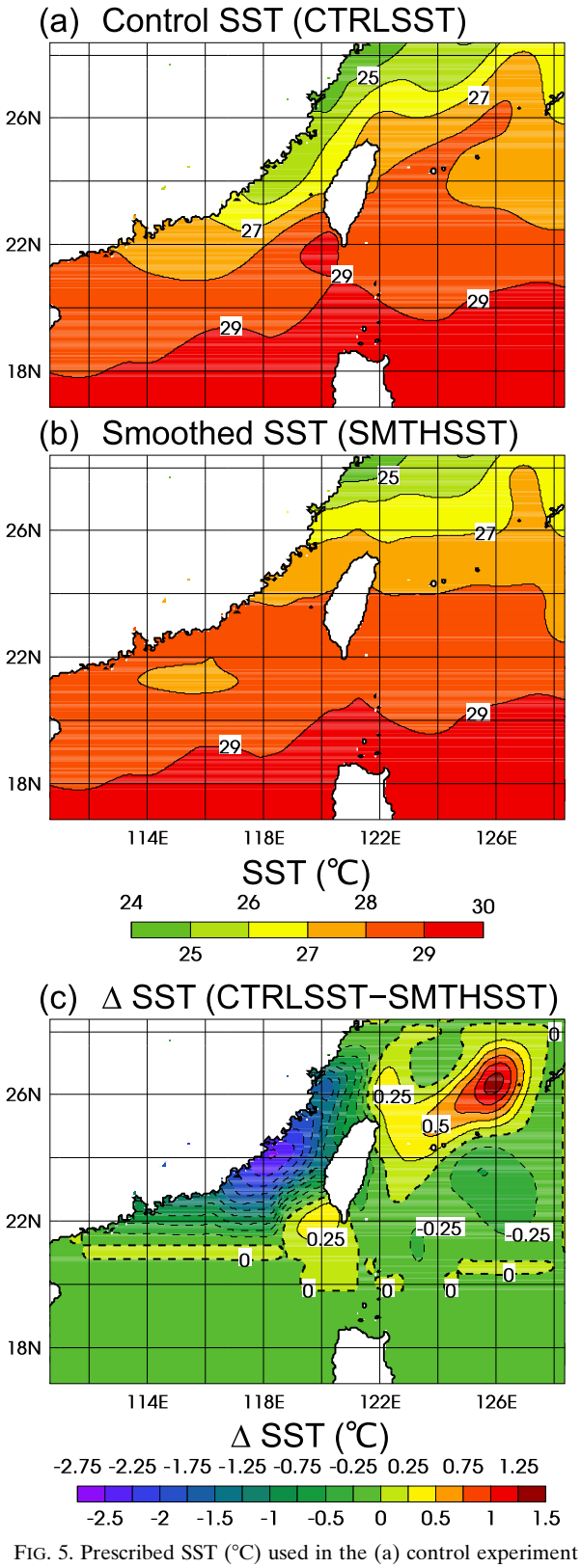

FIG. 5. Prescribed SST (°C) used in the (a) control experiment and (b) smoothed SST experiment. (c) SST difference (CTRLSST − SMTHSST). Extent of WRF Model domain is shown.

well as the topography, on the rainfall pattern during the period 13–18 June 2008. Two factors were considered in the experiments—the SST pattern in the SCS and the presence of the island of Taiwan. In all four experiments the model was initialized at 0000 UTC 12 June 2008 to allow the model to spin up. We provided the model with the observed 13–18 June-mean pattern shown in Fig. 5a for the control-SST (CTRLSST) runs and the pattern shown in Fig. 5b in which the SST gradient has been smoothed (SMTHSST). To smooth the SST field we used an ad hoc method of interpolating the SST along each meridian line between a southern point at ~20°N and a northern point at ~35°N (assuming a constant SST over land points along the northern latitude). This reduced the SST gradient to the southwest of Taiwan, and produced a somewhat zonally uniform profile. The SST is smoothed poleward of 20°–21°N, as shown by the difference between the two SST fields (CTRLSST − SMTHSST, Fig. 5c), and the smoothed field reverts to the observed values near the northern and eastern model boundaries. This step is undertaken to reduce the disequilibrium between the lower boundary and the lateral atmospheric boundary conditions prescribed by the NCEP analysis data. In the period 13–18 June of past years, such as 2002 and 2004 (Fig. 4d), the magnitude of the SST gradient in the Strait of Taiwan is not unlike that shown in the SMTHSST field (Fig. 5b). The smoothed field we generated, with the zonally aligned isotherms and Kuroshio warm tongue removed to the east of Taiwan, is admittedly not representative of a dynamically balanced ocean state, but rather it serves to produce an idealized situation where the southerly near-surface airflow is aligned with a weak SST gradient upstream of Taiwan (as observed in other past years) to contrast with the flow over the observed SST gradient. Similar modeling experiments, with smoothed SST fronts of the Kuroshio in the East China Sea, were carried out by Xu et al. (2011), Tanimoto et al. (2011), and Sasaki et al. (2012).

We repeated the CTRLSST and SMTHSST experiments with the island of Taiwan removed and replaced with ocean in order to test whether the rainfall sensitivity to SST with topography present is reproduced without topographic effects. The values of SST used in place of the island in the "NoTaiwan" (NT) experiments are interpolated values that come from the RTG SST dataset. The SST fields used in the experiments are shown in Fig. 6.

Table 1 shows a summary of the four experiments carried out. Each experiment consists of seven separate runs, each supplied with identical boundary forcing, but initialized with different atmospheric states. One run is initialized with the NCEP FNL Operational Global Analysis data directly interpolated to the model grid,

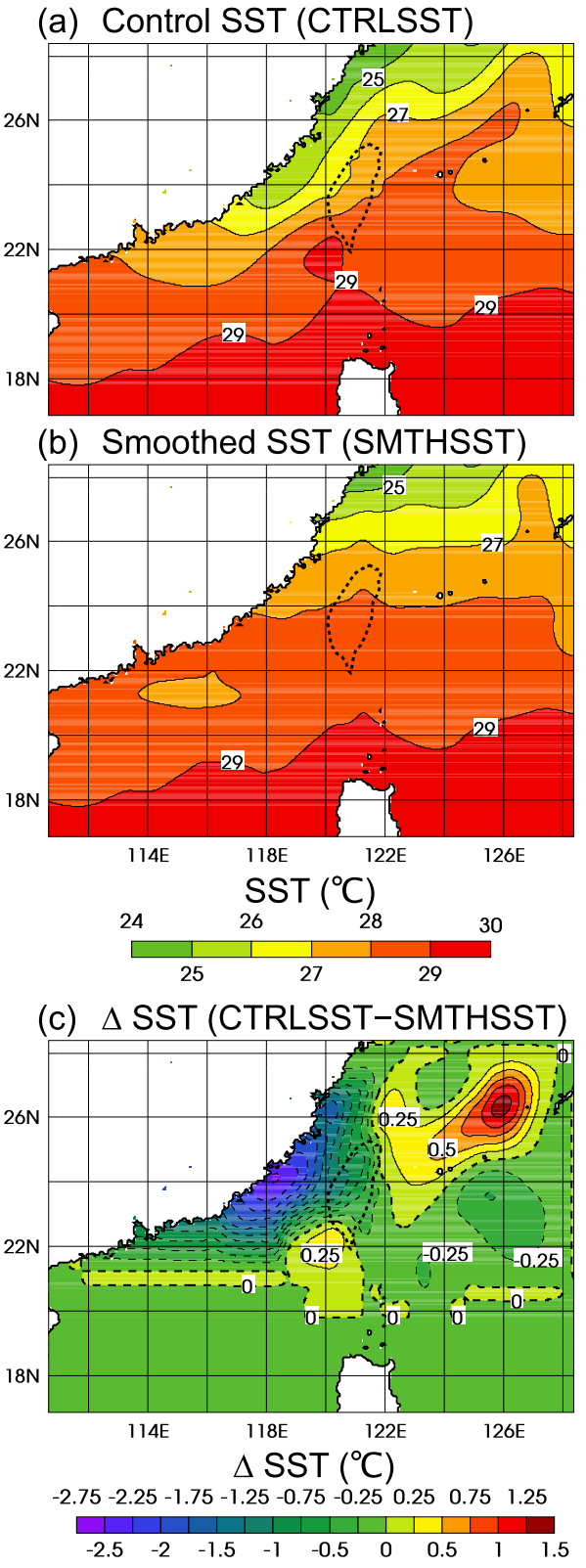

FIG. 6. As in Fig. 5, but with the island of Taiwan removed for the NoTaiwan experiments: position of Taiwan indicated by thick dashed line.

TABLE 1. Summary of the WRF modeling experiments performed.

Expt	SST pattern	Presence of Taiwan
SMTHSST-NT	Smoothed SST (Fig. 6b)	No
SMTHSST	Smoothed SST (Fig. 5b)	Yes
CTRLSST-NT	Observed SST (Fig. 6a)	No
CTRLSST	Observed SST (Fig. 5a)	Yes

and the remaining six runs are initialized with random perturbations calculated using the WRF Model data assimilation (WRFDA) system (Barker et al. 2004, 2012). The WRFDA system uses a three-dimensional variational data assimilation technique (3DVAR) to produce perturbations designed to maximize error growth and provide a reasonable ensemble spread. The same ensemble perturbations are applied in each of the four experiments. We found that, beyond three or four ensemble runs, the incremental changes to the ensemble-mean fields became diminishingly small, so we stopped at seven members as a representation of the climatology of possible outcomes for each of the separate lower boundary conditions. The results shown in this section are only the seven-member ensemble means for brevity. However, we should mention that each ensemble member making up the four experiments with the same initial perturbation produced similar sensitivities to the SST field, so the results of each member could support the conclusions made in this study. An advantage of analyzing the ensemble-mean fields is that the small-scale variations between the members are filtered out, producing information that provides a probabilistic view of the effects of the SST front.

a. Control run results

Figure 7a shows the WRF 13–18 June 2008 accumulated rainfall pattern from the control experiment, and over the large-scale region it is in general agreement with the TRMM observations (Fig. 7b). The zone of rainfall extending from the southern coast of China eastward to Taiwan is well represented, and the rainfall maximum over southern Taiwan is reproduced. The model places the maximum inland along the southwest coastline, which is in agreement with the QPE SUMS data (Fig. 3). The general rainfall distribution over Taiwan, with the northern half receiving less rain, is also in close agreement with QPE SUMS. The ensemble mean rainfall maximum of 450 mm on the southwest coast (Fig. 7a) is considerably less than the 550-mm maximum of the QPE SUMS data (Fig. 3). However, individual ensemble members have amounts comparable to the larger value (not shown).

The model also captures the temporal evolution of the rainfall event quite well. Figure 8 compares the daily

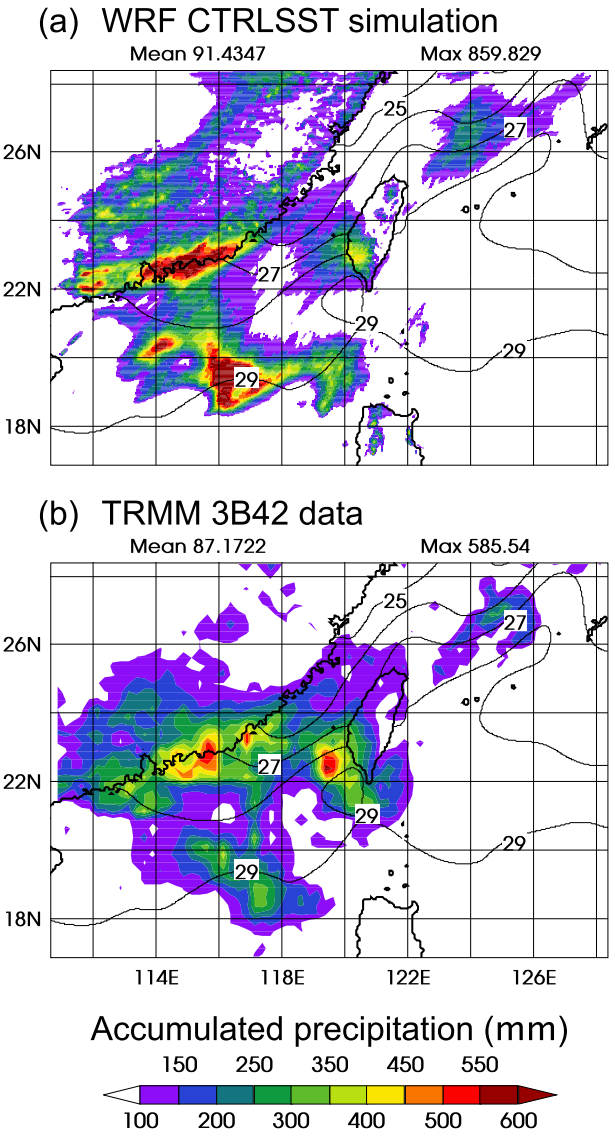

FIG. 7. Accumulated rainfall (color shading) over model domain from 0000 UTC 13 Jun through 0000 UTC 18 Jun from (a) WRF CTRLSST simulation and (b) TRMM 3B42 data. The SST (°C) is overlaid (contours).

rainfall pattern given by the model output and QPE SUMS data. Figure 9 is a time series of the 3-hourly rainfall averaged over the area shown by the box in Figs. 8i and 8j. As noted earlier, the first rain episode (14 June) was a squall line that propagated off the coast of China southeastward toward Taiwan. The second episode, on 16 June, formed just off the southwest coast of Taiwan and moved onshore. The simulated rainfall on 14 June is less than observed, and the model did not capture the break between the two episodes (Figs. 8 and 9). Instead, the model produces more rain on 15 June than on the prior day. Otherwise, the timing and intensity of the rainfall is similar between the model and observations.

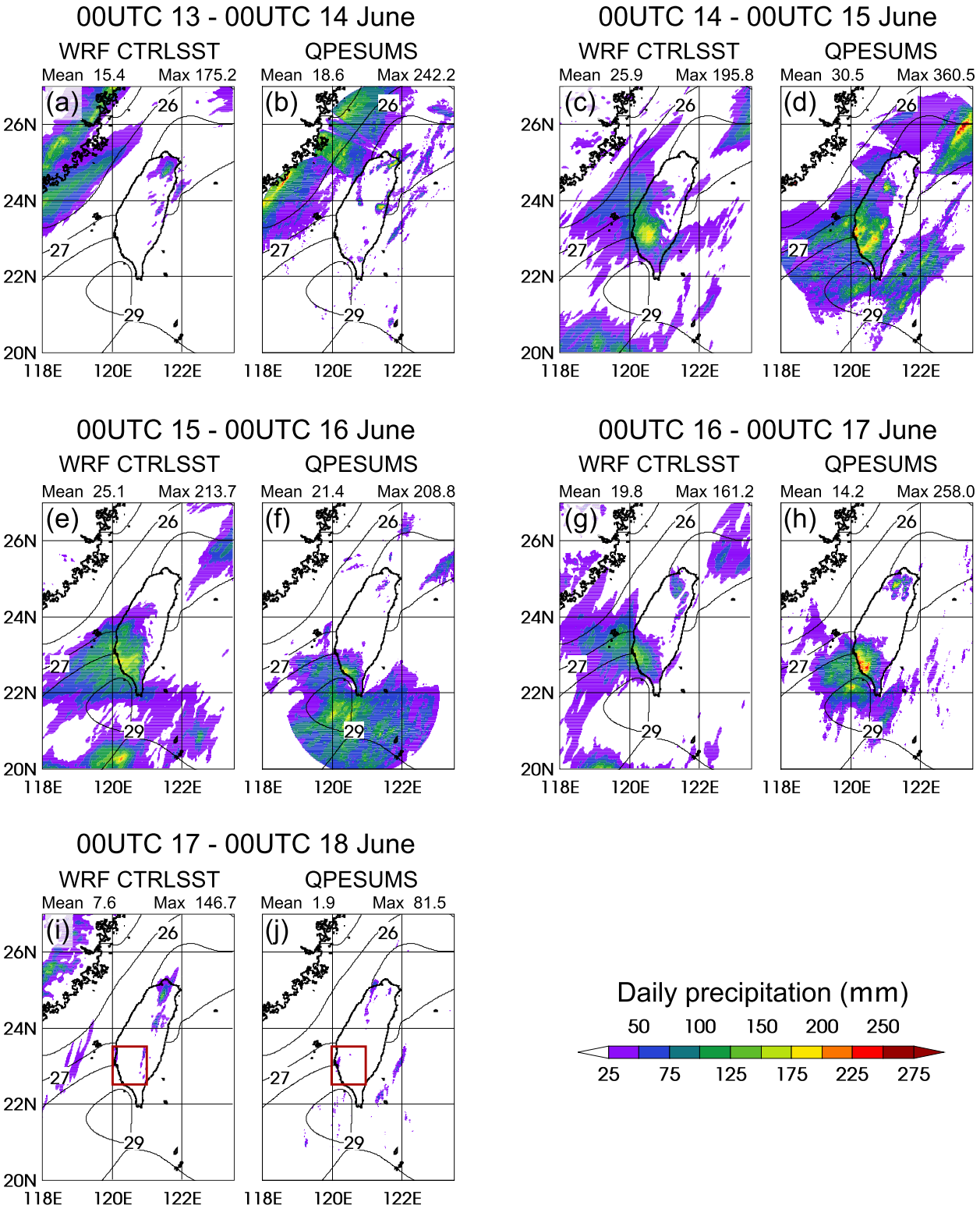

FIG. 8. Comparison of daily accumulated rainfall (mm) for 13–18 Jun 2008 between (a),(c),(e),(g),(i) WRF CTRLSST simulation and (b),(d),(f),(h),(j) QPE SUMS data. The SSTs are overlaid (contours). Boxes shown in (i),(j) indicate area used for rainfall time series.

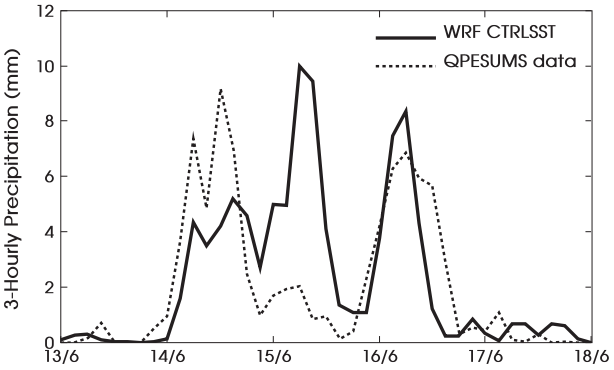

FIG. 9. Time series of 3-hourly precipitation averaged over the boxes shown in Figs. 8i,j comparing the CTRLSST simulation and QPE SUMS data.

b. Sensitivity to sea surface temperature

In this subsection we present the results of the SMTHSST experiment with the smoothed SST field shown in Fig. 5b. In this case, the low-level southerly flow overrides the same SST as in the CTRLSST experiment until about 21°N, when it encounters the smoothed SST gradient to the southwest of Taiwan. To show the effect of the change in SST (shown in Fig. 5c) on the simulated rainfall event and various aspects of the low-level flow, we will present difference plots of several fields between the CTRLSST and SMTHSST simulations. We should point out that, despite the fact that the SST smoothing covers a wide area (Fig. 5c), the gross features of the low-level flow near Taiwan, such as the location and intensity of the southwesterly jet, were not significantly altered by the smoothing. This is important because one could attribute differences in the rainfall fields to changes in the way the jet impinges on Taiwan, among other factors. Since we smoothed the SST only northward of ~21°N and the flow is generally southerly from the surface to approximately 200 hPa in height at this latitude, we expect the main effect on the low-level air to be the local difference in SST gradient to the southwest of Taiwan: that is, the feature of interest.

1) EFFECT ON RAINFALL

Figure 10a shows the 13–18 June simulated rainfall from the SMTHSST experiment. Over southwestern coastal Taiwan there is still a large rainfall maximum; however, it is reduced compared to that of the CTRLSST simulation (Fig. 7a). The difference in the rainfall amount between the CTRLSST and SMTHSST experiments is shown in Fig. 10b. There is a general correlation between the rainfall and SST differences, particularly over the warmer waters of the SMTHSST field to the west of the northern part of the island. However, in the vicinity of the strong SST fronts in the CTRLSST field off the southwest coast

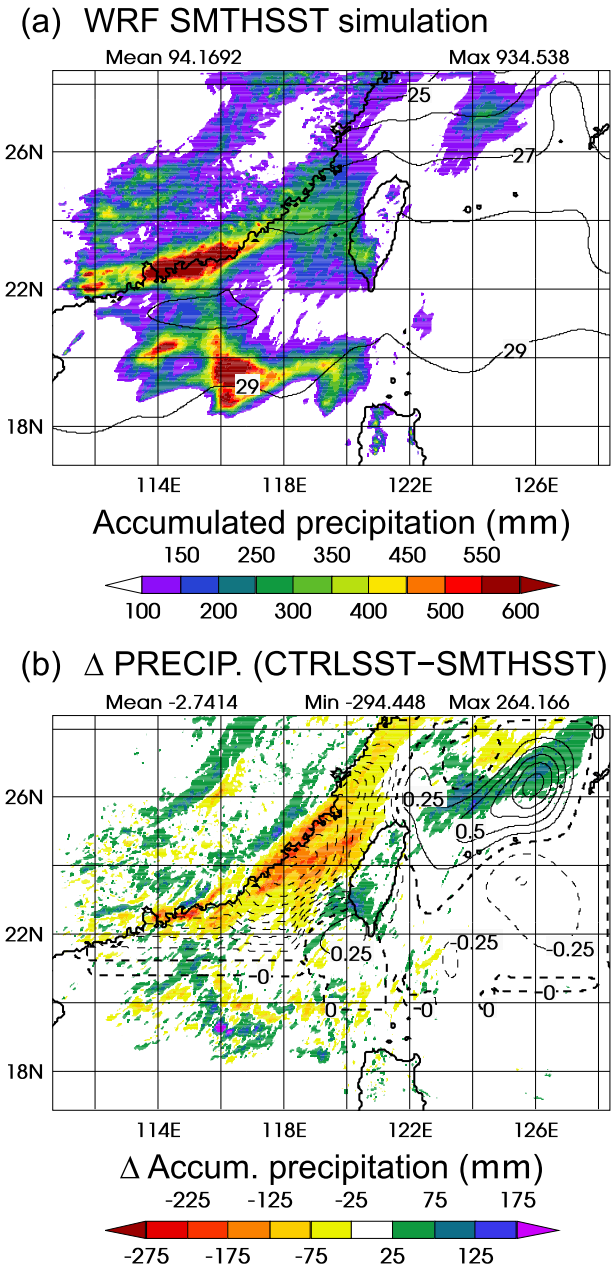

FIG. 10. (a) Accumulated rainfall (color shading) over model domain from 0000 UTC 13 Jun through 0000 UTC 18 Jun from WRF SMTHSST simulation. SST (°C) is overlaid (contours). (b) Rainfall difference (color shading) between CTRLSST and SMTHSST simulations. SST difference between CTRLSST and SMTHSST simulations is overlaid (0.25°C contour interval with negative values indicated by dashed lines).

of Taiwan and to the northeast of the island along latitude 26°N (Fig. 5a), the rainfall difference maxima (green and blue shading in Fig. 10b) are located northward of the SST difference maxima, which indicates that the heavier rainfall of the CTRLSST case in these regions is related to the SST gradient rather than to

warmer waters. Over southwestern Taiwan, the maximum rainfall amount for the SMTHSST case is 385 mm, which is a 65-mm reduction from the CTRLSST case (cf. Figs. 7a and 10a), indicating that the sharp SST gradient had a considerable positive effect on the intensity of the heavy rainfall event. The areal-averaged accumulated rainfall over the region shown by the box in Figs. 8i and 8j is 21% higher in the CTRLSST experiment (93.9 mm) than in the SMTHSST experiment (77.3 mm).

2) Effect on buoyancy fluxes and PBL structure

Mesoscale SST fronts impact air–sea surface fluxes as surface winds flow from either cold to warm or warm to cold SSTs (e.g., de Szoeke and Bretherton 2004; Skyllingstad et al. 2007). As the low-level flow encounters such fronts, the air comes out of equilibrium with the sea surface, and modified turbulent exchanges occur across the lower boundary. In the case of the East Asian summer monsoon near Taiwan, the southerly flow brings warm air over colder waters and results in a transfer of sensible heat to the ocean. In the moist PBL, the surface buoyancy flux F, which influences the growth of the boundary layer, can be written $F = S + 0.61 c_p T_S E/L$, where S is the sensible heat flux, E the latent heat flux, T_S the surface skin temperature, L the latent heat of vaporization, and c_p is the specific heat of dry air at constant pressure (Stull 1988, p. 147). The simulated sea surface buoyancy flux for the control run is shown in Fig. 11a. Over the warmer waters to the south, the buoyancy fluxes are large, and presumably the PBL is well mixed in these regions. To the north, over the colder waters, the buoyancy flux decreases substantially, becoming negative off the coast of southeastern China.

The presence of small and negative buoyancy fluxes over the northern South China Sea shown in Fig. 11a is consistent with comparable fluxes measured during the South China Sea Monsoon Experiment (SCSMEX) in 1998, as described by Ciesielski and Johnson (2009). Ciesielski and Johnson documented a high frequency of stable boundary layers (relative to other regions of the tropics) observed over the northern SCS and correlated these to small buoyancy fluxes measured over the colder waters north of the SST gradient.

During TiMREX, surface fluxes were not measured, but sounding data can be used to determine the stability of the PBL and to infer the existence of a horizontal gradient of buoyancy fluxes across the SST front as simulated by the WRF. Figure 12 compares radiosonde and model potential temperature profiles below 850 hPa at two locations that straddle the SST front, as shown in Fig. 11a. The northern soundings were taken from Makung island (Station 46734), and the southern soundings were

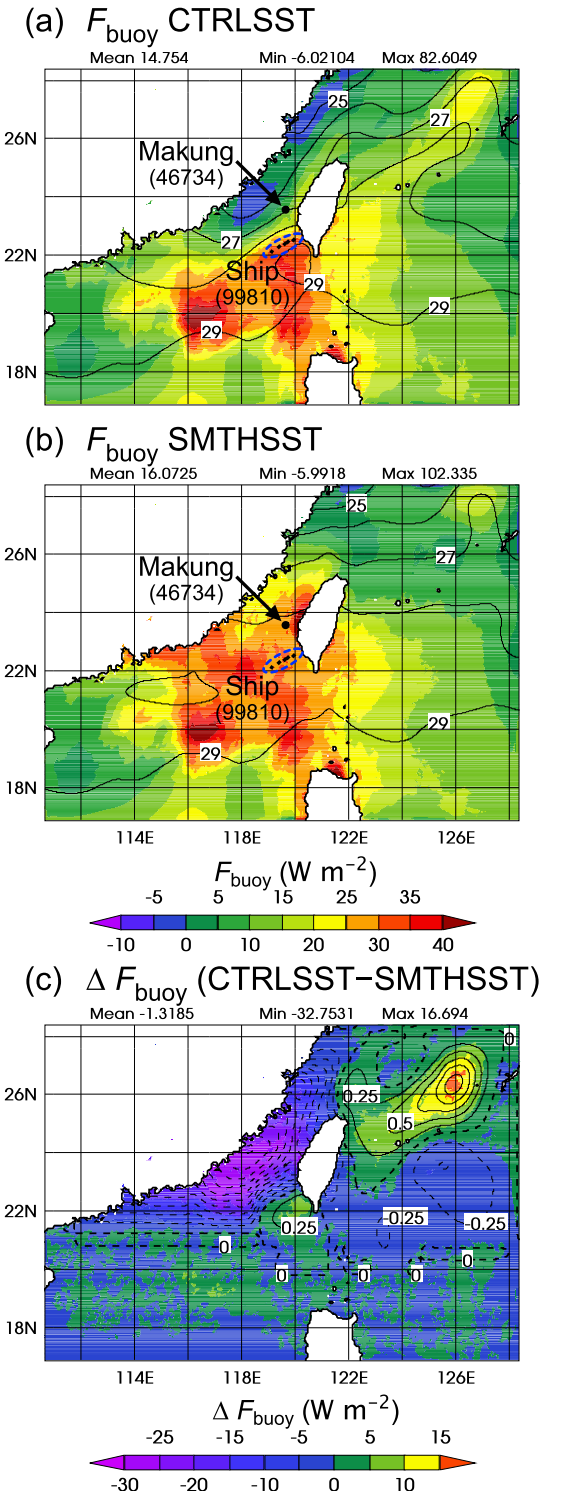

FIG. 11. Mean 0000 UTC 13 Jun–0000 UTC 18 Jun buoyancy flux (color shading) for (a) CTRLSST and (b) SMTHSST simulations with SSTs (°C) overlaid (contours). (c) Buoyancy flux difference between CTRLSST and SMTHSST simulations with SST difference (CTRLSST − SMTHSST) overlaid (0.25°C contour interval with negative values indicated by dashed lines). Locations of Makung Island (46734) and ship (99810) (multiple locations enclosed by oval) radiosonde stations are shown in (a),(b).

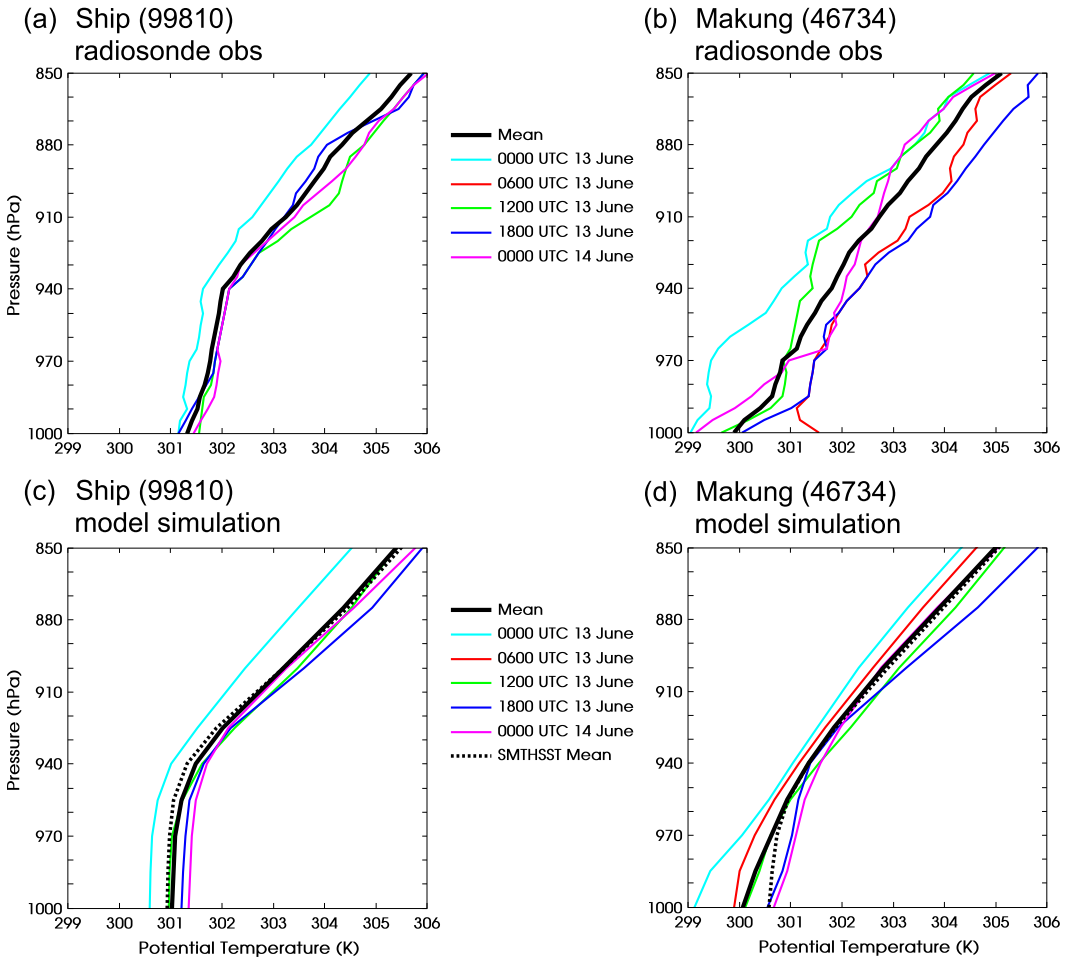

FIG. 12. Vertical potential temperature profiles based on (a),(b) 6-hourly radiosonde data and (c),(d) model profiles from corresponding grid points and times from the WRF CTRLSST simulation. Mean profiles from the SMTHSST simulation are shown by thick dashed curves in (c),(d).

from the research vessel, with multiple locations during the period of study (Figs. 11a,b). While the Makung sounding station is located on land, we found that the soundings are representative of ocean soundings when compared to nearby dropsondes over water (not shown). Since the station is within 1 km of the windward (southern) coast of the island and the intervening vegetation is rather low, the PBL is presumably not greatly affected by the land surface. The 6-hourly soundings shown are from the 24-h period beginning 0000 UTC 13 June and ending 0000 UTC 14 June 2008 (the 0600 UTC ship sounding was not included due to data quality issues). This period preceded the rainfall passage and was chosen to show that the low-level convergent flow was preconditioned by the SST gradient to favor precipitation. Figure 12 indicates that in both the observations and the model, the PBL was approximately well mixed over the warm waters to the south and was stable over the colder waters to the north of the SST front, confirming the strong gradient in buoyancy flux across the front shown in Fig. 11a. Figure 13 gives a similar picture from the standpoint of wind speed. The higher wind shear on the north side of the front indicates a stable PBL, and the slower near-surface wind speeds, compared to the southern site, suggest an enhancement to low-level convergence associated with the SST front.

In general, the WRF Model profiles are in remarkably close agreement with the radiosonde data. There is a striking difference, however, in the lowest 10 hPa (~100 m) of the ship profiles. The radiosonde data suggests that there is a stable surface layer, which is absent in the WRF profiles. We cannot account for this discrepancy, but the agreement of the profiles above 100 m indicates that the WRF Model accurately represents the observed PBL structure.

The difference between the soundings at the two locations supports the vertical-mixing mechanism of

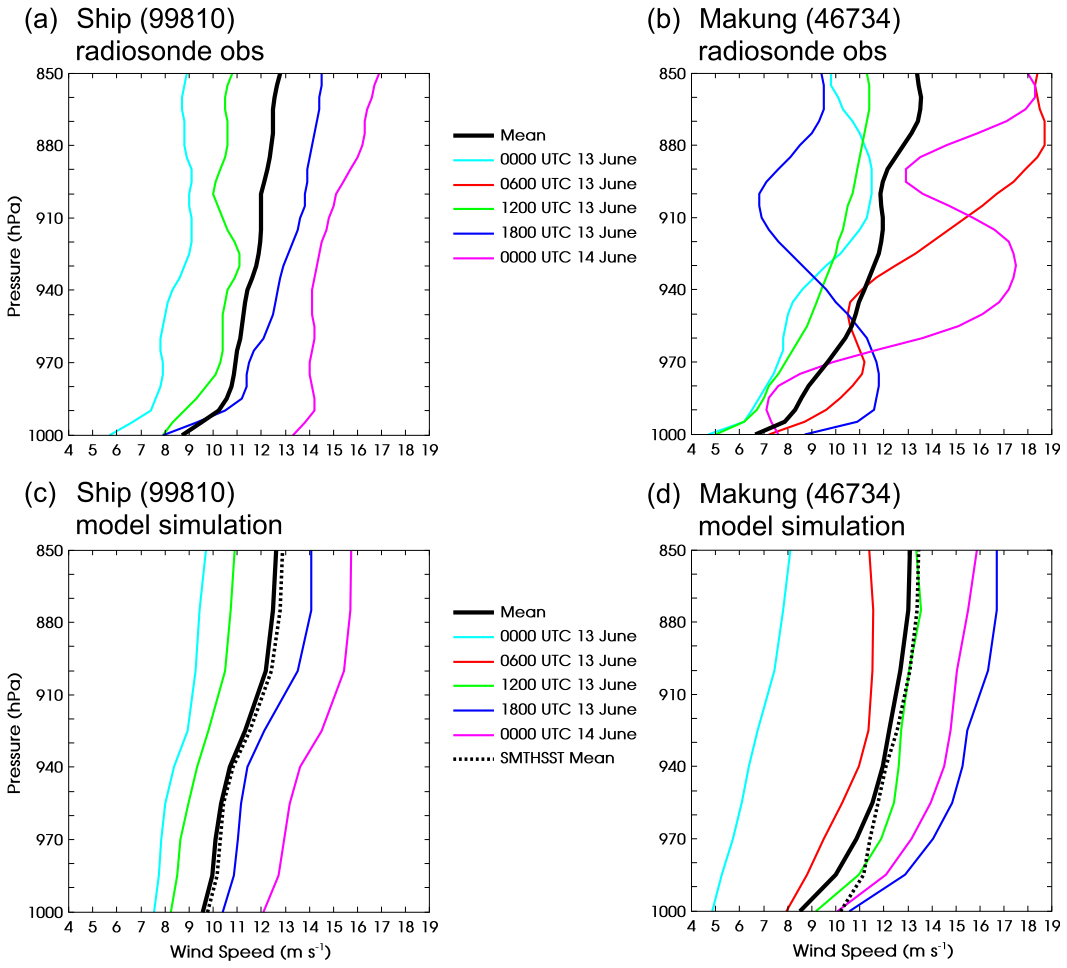

FIG. 13. Vertical wind speed profiles based on (a),(b) 6-hourly radiosonde data and (c),(d) model profiles from corresponding grid points and times from the WRF CTRLSST simulation. Mean profiles from the SMTHSST simulation are shown by thick dashed curves in (c),(d).

Wallace et al. (1989): namely, downward vertical mixing of southerly momentum is reduced as air flows from warm to cold SST, hence leading to surface convergence. Figures 12 and 13 also show the mean vertical profiles from the SMTHSST model simulations. In the southern (ship) locations, the SST is about the same as in the CTRLSST case, and the mean soundings are almost the same in both simulations. However, in the northern location (Makung), the PBL is less stable (more mixed) in the SMTHSST case. We will show that this structure is tied to weaker convergence and decreased rainfall in the SMTHSST simulation.

As mentioned above, the preconvection PBL profiles are shown to suggest that the horizontal gradient in vertical mixing associated with the SST front enhances the triggering of convection. During the subsequent precipitation events that occurred from 14 June through 17 June, the mean soundings at the two locations (not shown) indicate that the well-mixed and stable PBL structures at the southern and northern locations, respectively, were generally maintained. Therefore, the vertical-mixing mechanism likely continued to play a role in enhancing precipitation, despite the flow perturbations to the mean flow caused by the convective systems themselves.

With the smoothed SST field at the lower model boundary, the buoyancy fluxes are positive throughout Taiwan Strait (Fig. 11b), suggesting that with a weaker SST front the PBL would be well mixed throughout. Without the northward transition to a stable boundary layer, an anomalously convergent low-level flow would not occur. This hypothesis will be supported in the following discussion. Figure 11c shows that there is a strong correlation between the difference in SST and buoyancy flux between the two simulations.

3) Effect on low-level flow and horizontal convergence

Figure 14 shows the mean 13–18 June horizontal divergence fields at 985 hPa produced by the WRF Model experiments. The data were filtered with a 10-point Gaussian smoother to eliminate noise. In both CTRLSST and SMTHSST simulations (Figs. 14a and 14b, respectively), there are convergence maxima just off the southwest Taiwan coast, which correspond to regions of heavy coastal rainfall (Figs. 7a and 10a, respectively). The rising motion tied to the low-level convergence presumably enhances convective rainfall. The convergence maxima upwind of the island barrier are likely due mainly to terrain blocking effects (e.g., Wang et al. 2005); however, the difference in low-level divergence between the two experiments (CTRLSST minus SMTHSST, Fig. 14c) shows that the low-level convergence is enhanced in the CTRLSST flow over the sharp SST front off the southwest Taiwan coast. We propose that this enhancement is a result of the mechanism described by Wallace et al. (1989), whereby the transition from a mixed to stable PBL causes low-level winds to decelerate (owing to reduced downward mixing of high-momentum air from aloft).

To examine the effect of the SST front on the near-surface atmosphere, we consider a vertical cross section along the 120°E longitude line from 20° to 26°N (see Fig. 14), which is approximately aligned with the low-level wind. Figure 15 presents the vertical flow profiles with the two SST patterns, as well as the difference (CTRLSST − SMTHSST) in various fields between the two experiments. The contour plots in Figs. 15a–d are time averages over the 24-h period from 0000 UTC 13 June to 0000 UTC 14 June, prior to the heavy rainfall episode of 14 June (see Figs. 8a,b and 9). The low-level jet, whose core is situated above 850 hPa and just beyond the northern extent of the profiles, is seen in the plots of wind speed shown in Figs. 15a,b. In the CTRLSST experiment (Fig. 15a), the low-level wind shear strengthens considerably northward (downwind) of about 23°N where the SST front is located (see Fig. 15e). Note that the near-surface (lowest 15 hPa) wind speed actually decreases in a narrow region from roughly 22.8° to 23.3°N. The wind shear increase, and associated decrease in the surface wind speed (Fig. 15a), coincides with the northward transition from a well-mixed to a stable boundary layer, which, in turn, is caused by a steep drop-off in the buoyancy flux (Fig. 15e). The transition in PBL stability is clearly evident in the potential temperature profile in Fig. 15c. Note that the two soundings shown in Figs. 12 and 13, whose locations straddle the SST front close to 120°E, are represented in these vertical profiles, which show the transition from a well-mixed to stable PBL

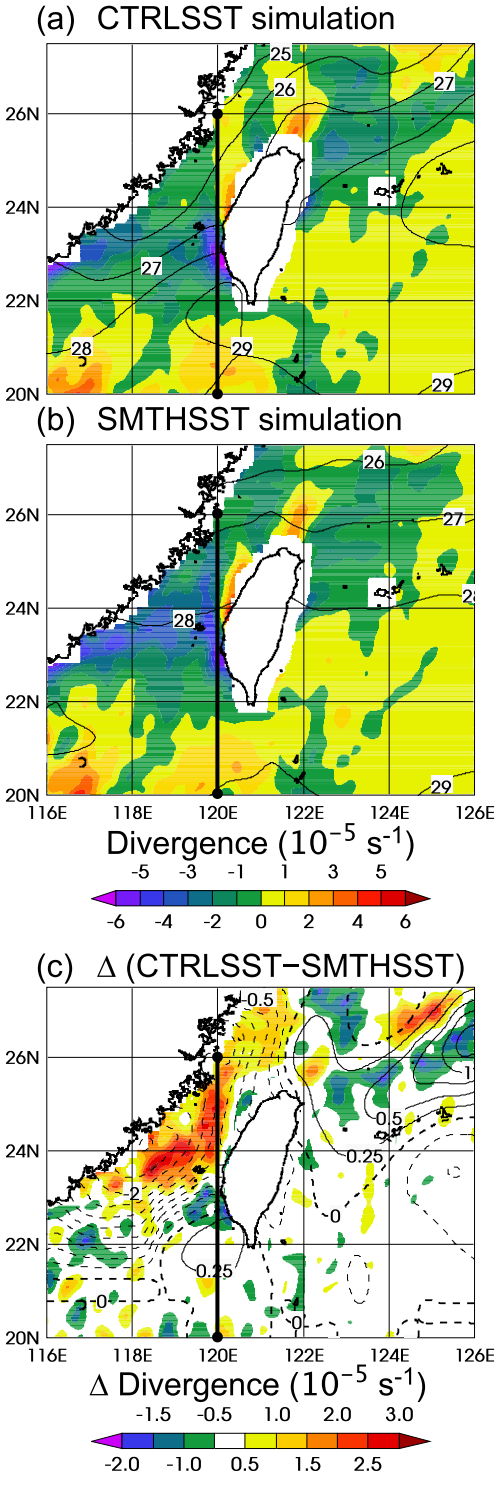

FIG. 14. Mean 13–18 Jun horizontal divergence at 985 hPa (color shading) from (a) CTRLSST and (b) SMTHSST simulations with SSTs (°C) overlaid (contours). (c) Difference in 985-hPa horizontal divergence between CTRLSST and SMTHSST simulations with SST difference (°C) overlaid (0.25°C contour interval with negative values indicated by dashed lines). Position of the vertical cross section along 120°E is shown by the thick black lines.

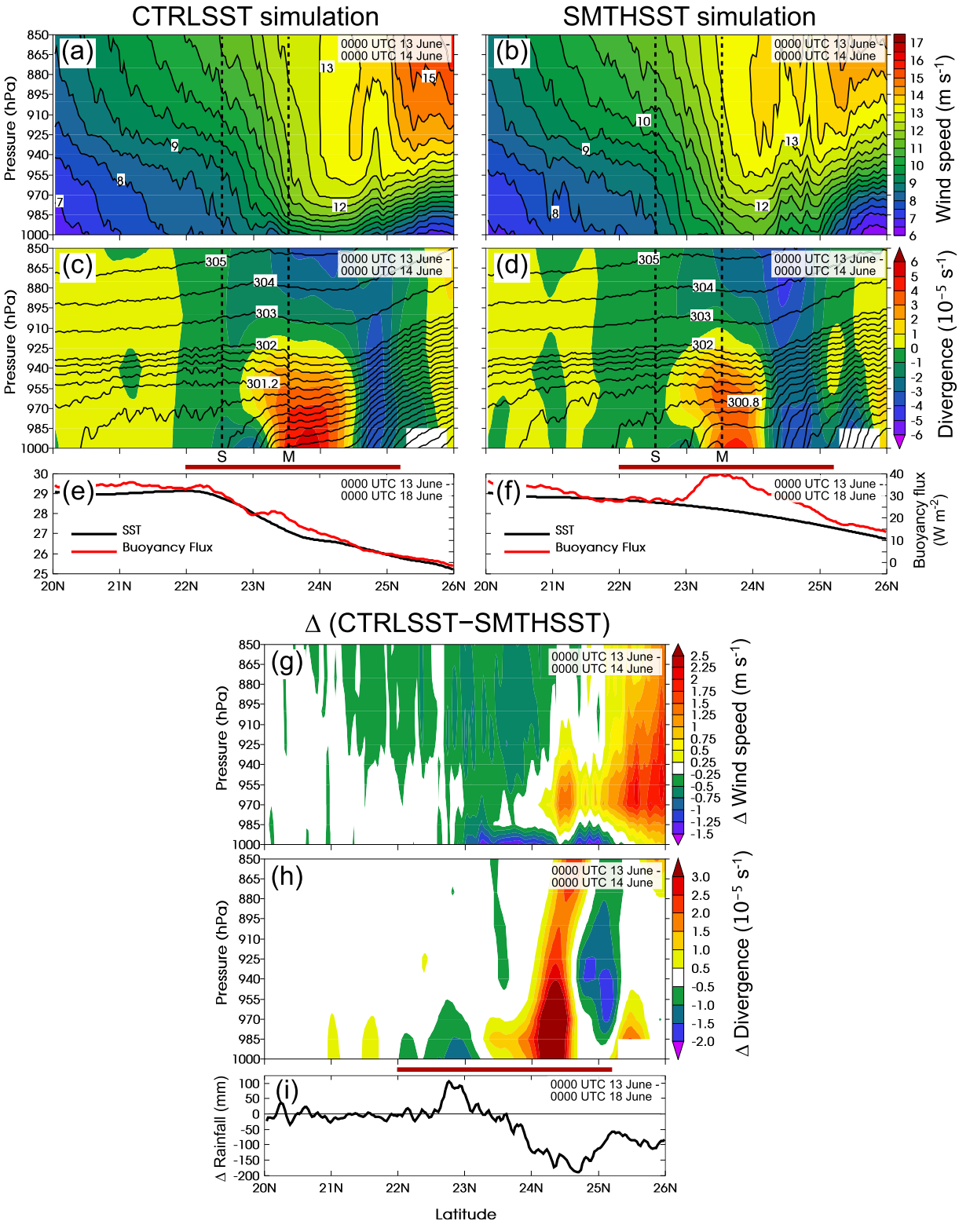

FIG. 15. Vertical cross sections along 120°E of mean 0000 UTC 13 Jun–0000 UTC 14 Jun (a),(b) wind speed, (c),(d) horizontal divergence (color shading) and potential temperature (K) (contours, with 0.2-K interval for $\theta \leq 302$ K), and difference (CTRLSST − SMTHSST) in (g) wind speed and (h) horizontal divergence. (e),(f) Mean 0000 UTC 13 Jun–0000 UTC 18 Jun buoyancy flux (red curve) and SST (black curve) along 120°E. (i) Difference (CTRLSST − SMTHSST) in accumulated rainfall along 120°E from 0000 UTC 13 Jun through 0000 UTC 18 Jun. Letters "S" and "M" indicate the latitude of ship (99810) and Makung (46734) radiosonde stations, respectively. The thick brown line indicates the latitude range of the island of Taiwan for reference.

suggested earlier by the two soundings. We also note that the vertical profiles closely resemble those presented in an idealized modeling study by Skyllingstad et al. (2007) of flow over a SST front from warm to cold water.

A region of low-level convergence exists along 120°E off the coast of southern Taiwan from about 22° to 23.3°N (Fig. 15c), bordered on the north by a region of strong divergence (from about 23.3° to 24.5°N). These features are characteristic of the barrier jet that forms to the west of the island owing to flow blocking (e.g., Li and Chen 1998; Yeh and Chen 2002; Wang et al. 2005). The main portion of the convergence in the upwind feature is due to the westward deflection of the flow away from the topography. However, a portion of the convergence is due to the deceleration of the flow in the northward direction resulting from the SST front, as mentioned above. The results of the SMTHSST experiment show that, with the weaker SST front (Fig. 15f) and in the absence of a drop-off in the surface buoyancy flux (Fig. 15f), the surface winds do not decelerate as strongly as in the CTRLSST case (cf. Figs. 15a,b) near 23°N and that the potential temperature profile remains somewhat well mixed. Figure 15g shows the dramatic near-surface wind speed decrease of the CTRLSST case compared to SMTHSST northward of 23°N. Figure 15h shows the difference in horizontal divergence between the CTRLSST experiment (Fig. 15c) and the SMTHSST experiment (Fig. 15d). The enhancement of convergence for the CTRLSST case in the lowest 30 hPa just southward of 23°N (Fig. 15h) is due mainly to the near-surface wind deceleration as the vector difference between the flows (CTRLSST − SMTHSST) is oriented in the opposite direction of the flow.

The contrasts in the low-level flow profiles confirm the links between SST gradients, PBL stability, and gradients in the vertical mixing of momentum as proposed by Wallace et al. (1989). This mechanism explains the enhanced low-level convergence (and resulting vertical motion) due to the sharp SST front, and it likely contributed to the enhancement of the 13–18 June 2008 heavy rainfall event. Figure 15i shows the difference (CTRLSST − SMTHSST) in the 13–18 June 2008 rainfall. Note that the local maximum of 100 mm just south of 23°N coincides with the enhanced convergence previously described (Fig. 15h). As mentioned earlier, recent studies have linked PBL modification by strong mesoscale SST gradients to enhanced convective precipitation in various parts of the world (e.g., Minobe et al. 2008; Xu et al. 2011; Li and Carbone 2012; Miyama et al. 2012). Over the northern SCS during the onset of the East Asian summer monsoon, the troposphere is very moist and conditionally unstable, so it is expected that convection would be particularly sensitive to the additional triggering mechanism offered by a sharp SST front.

To support our earlier suggestion, based on radiosonde observations, that the differential mixing of momentum continued to exist across the SST gradient during the convectively active period, we consider vertical profiles, shown in Fig. 16, averaged over the 3-day rainy period from 0000 UTC 14 June to 0000 UTC 17 June (refer to Figs. 8c–h and 9). There is a striking difference in the divergence fields of Figs. 16c and 16d compared to those of the preconvective period (Figs. 15c,d) in that the region from 21.5° to 25°N is entirely convergent because of the convection. However, the convergence difference between the CTRLSST and SMTHSST simulations (Fig. 16f) is remarkably similar to that of the preconvective period (Fig. 15h) over the SST front just southward of 23°N, which again corresponds to the increased rainfall amount shown in Fig. 15i. We suggest that the enhanced convergence is a causal factor on the enhanced convection because the PBL potential temperature and wind speed structures, which were formed owing to the SST gradient during the preconvective period (Figs. 15a–d), remain evident during the rainy period (Figs. 16a–d): that is, the PBL becomes more stable crossing the SST front northward from 22.5° to 23.5°N in the CTRLSST simulation versus the SMTHSST simulation (Figs. 16c,d); correspondingly, the mean low-level flow decelerates across the front in a similar manner to the preconvective period (cf. Figs. 16e and 15g).

It is striking that a well-mixed mean PBL potential temperature profile is maintained in the southern portion of the SST front (~22.5°N) during the convectively active period (Fig. 16c). In both sounding and model data (not shown), stable PBL profiles develop during precipitation events, but a well-mixed profile is quickly restored after the convection has passed. The reason for this is likely because of the relatively warmer SST south of the front, which facilitates the recovery of a well-mixed PBL, as well as the strong southerly flow, which continually advects warm, undisturbed low-level air into the region.

The pressure-adjustment mechanism proposed by Lindzen and Nigam (1987) for modification of the low-level flow by large-scale SST gradients also appears to contribute to the perturbed flow field over the broad area of the northern SCS. Their theory assumes that SST anomalies affect mainly the lowest levels of the atmosphere and that near-surface hydrostatic pressure perturbations develop as a result of the varying SST. Figure 17 shows the difference in geopotential height and horizontal winds between the CTRLSST and SMTHSST

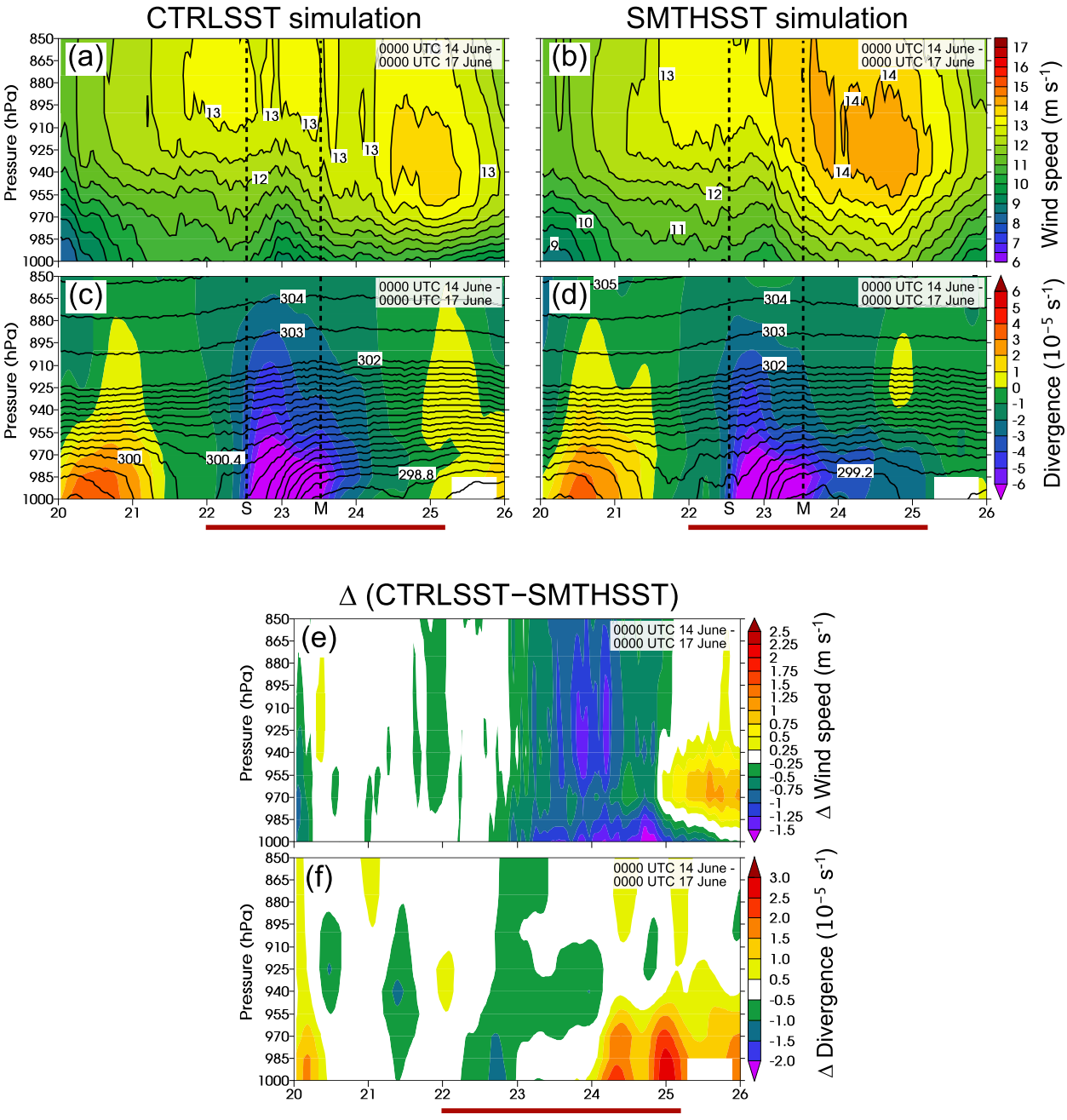

FIG. 16. (a)–(d) As in Figs. 15a–d and (e),(f) as in Figs. 15g,h, but time averaged over the period 0000 UTC 14 Jun–0000 UTC 17 Jun.

simulations at 1000 hPa and 850 hPa averaged over the period 0000 UTC 13 June to 0000 UTC 18 June. The perturbation geopotential at 850 hPa are indeed smaller than those at 1000 hPa, and the signs of the perturbations agree with the pressure-adjustment theory of Lindzen and Nigam in that over the colder (warmer) waters of the CTRLSST, the geopotential height is slightly higher (lower) than that of the SMTHSST simulation (cf. Fig. 5c). At 850 hPa, the perturbation wind vectors qualitatively appear to be in geostrophic balance with the perturbed height field, while at 1000 hPa the perturbation winds flow to a significant degree down the pressure gradient. Note that the perturbation wind vector fields are consistent with the perturbation divergence fields of Fig. 14c. Previous modeling studies on the effects of SST fronts on low-level flow have included quantitative momentum budget analyses to assess the relative contributions of the pressure-adjustment versus vertical-mixing mechanisms

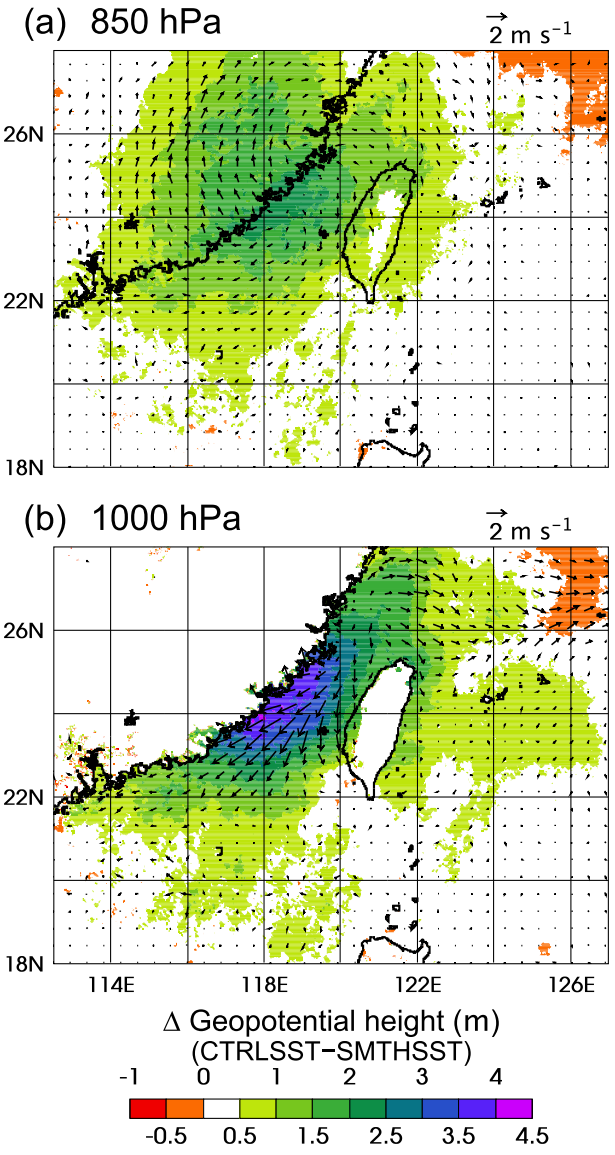

FIG. 17. Difference (CTRLSST − SMTHSST) in geopotential height (m) (colored shading) and winds ($m\,s^{-1}$) at (a) 850 and (b) 1000 hPa averaged over the period 0000 UTC 13 Jun–0000 UTC 18 Jun.

(e.g., Bourras et al. 2004; Kuwano-Yoshida et al. 2010; O'Neill et al. 2010) and found that both processes can be important in accelerating the flow.

c. *Simulations with Taiwan removed*

To separate the effects of the SST front on the rainfall from the island orographic effects, we repeated the experiments with the two SST fields but with the island of Taiwan removed and replaced with ocean. Sea surface temperature data over the missing island were supplied by the RTG SST dataset (Fig. 6). We will compare the sensitivity to the change in SST between the CTRLSST and SMTHSST patterns with the island removed to the results found in the previous subsection. If the sensitivity is similar to that with the island in place, it will support our argument for the enhancement of rainfall over coastal Taiwan owing to the existence of the sharp SST front.

Looking at the mean 13–18 June low-level divergence fields, Fig. 18a shows that there is still strong convergence over the SST front corresponding to the location of the southwest coast of Taiwan; however, it is not as strong without the blocking effect of the island topography (Fig. 14a). With the smoothed SST field, the convergence in the same location is greatly reduced (Fig. 18b). The difference field (CTRLSST − SMTHSST) shown in Fig. 18c displays a remarkably similar pattern off the southwest Taiwan coast as with the island in place (Fig. 14c). The effect of the SST field on the low-level convergence is, therefore, qualitatively independent of the presence of the island. In addition, the vertical profiles along the same cross section as in the previous subsection, and the inferences regarding the role of vertical mixing across the SST front, are almost the same with the island removed, as shown in Fig. 19 compared to Fig. 15. In particular, we see a similar deceleration of the near-surface winds just north of 23°N and a corresponding increase in the convergence of the lowest 30 hPa (Figs. 19g,h). As in the case with the island in place, this is due to a transition from a mixed PBL to stable PBL across the SST front in the CTRLSST experiment, as indicated by the horizontal wind speed and potential temperature fields shown in Figs. 19a and 19c, respectively. As before, the enhanced accumulated rainfall at 23°N along the cross section (Fig. 19i) corresponds to the enhanced low-level convergence (Fig. 19h), and it almost reaches the same maximum of 100 mm. As an aside, note that with the absence of the island topography there is no barrier jet evident in the wind speed and divergence fields (cf. Figs. 15a–d and 19a–d).

Figure 20 shows the vertical profiles during the convectively active period from 0000 UTC 14 June to 0000 UTC 17 June. As in the case with the island of Taiwan present, the horizontal gradient of vertical momentum mixing in the PBL owing to the sharp SST gradient is still a factor during the rainy episode. This is evidenced by the enhanced low-level convergence near 23°N (Fig. 20f) similar to that of the preconvective period (Fig. 19h), reduction of low-level wind speed northward of 23°N (cf. Figs. 20e and 19g), and a much stronger transition from a mixed to stable PBL northward across the front from 22.5° to 23.5°N when comparing the potential temperature fields of Figs. 20c and 20d.

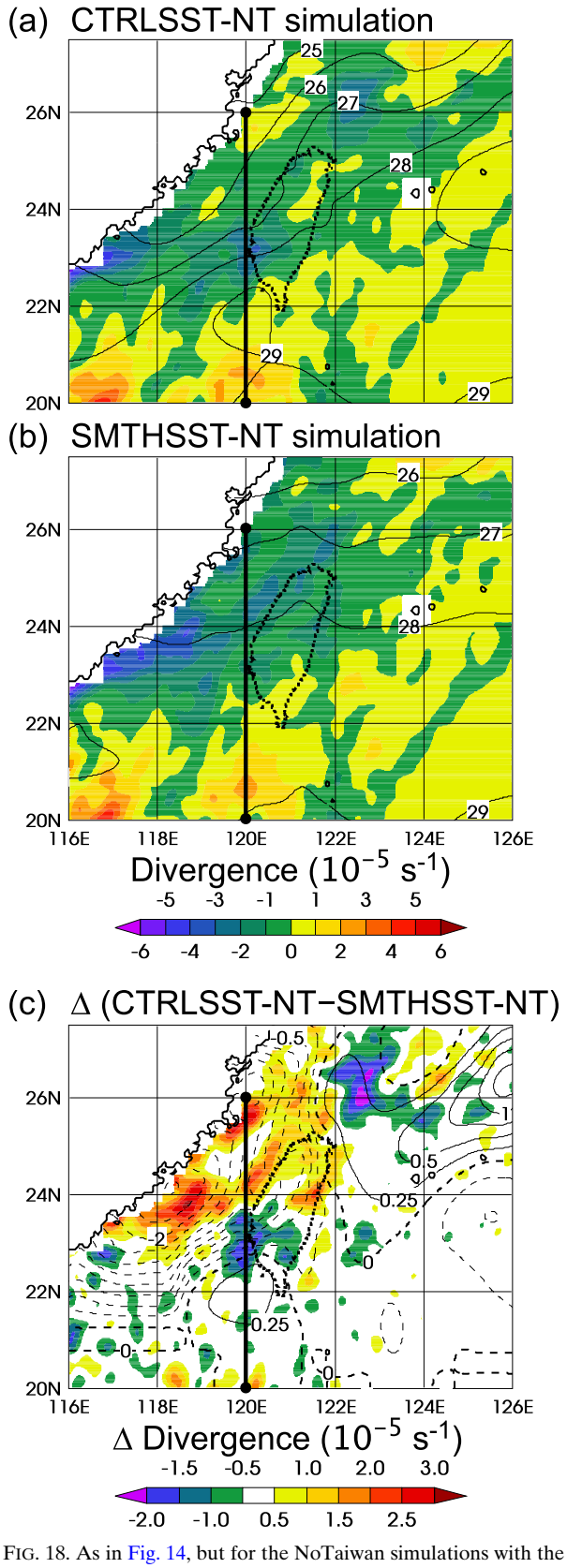

FIG. 18. As in Fig. 14, but for the NoTaiwan simulations with the island of Taiwan removed.

The accumulated rainfall for 13–18 June for the NoTaiwan case is shown in Fig. 21. Similar to when the island is present, the CTRLSST rainfall (Fig. 21a) coincides well with the sharp SST gradient and the strong low-level convergence. The sensitivity to the SST field exhibits a similar pattern as with the island in place (cf. Figs. 21c and 10b). This means that the effect of the SST pattern is somewhat independent of whether the island is there or not. We will examine this behavior in the following subsection. It is also interesting to note that without the island, there is still a rainfall maximum off the southwest coast of the missing island (Fig. 21a), which is greatly reduced in the SMTHSST case (Fig. 21b). Therefore, the southwest coast of Taiwan was prone to extreme rainfall owing to both the blocking effect of the island and the SST front.

d. Factor separation analysis: Comparing the roles of the SST front and island topography on rainfall

In the previous subsections we examined the sensitivity of the simulated rainfall to changes in two factors—the presence of a strong SST front and the presence of the island of Taiwan. In this subsection we apply the formalized technique known as factor separation analysis (Stein and Alpert 1993; Alpert et al. 1995; Alpert and Sholokhman 2011; Seigel et al. 2013) to isolate the effects of the two factors individually, as well as to reveal the synergy between them. The similarity between the rainfall difference fields shown in Figs. 10b and 21c suggests that the effect of the topography of Taiwan on the PBL modification by the SST front is small: that is, the synergy between the two factors is small. This indicates the robustness of the role of the SST front on rainfall patterns in the vicinity of Taiwan.

The concept of synergy in factor separation analysis refers to the nonlinear interaction of multiple factors. In this paper, we have argued that the effect on rainfall by the SST front occurs mainly through the PBL modification of the overlying airflow via the vertical-mixing mechanism of Wallace et al. (1989). We should expect the degree of PBL modification to be affected by the wind speed and direction across the front, which itself is affected by the presence of the island topography. Similarly, the topographic effects of the island are sensitive to the wind speed and direction, which are affected by the upwind SST pattern. How strongly these factors interact is the synergy.

We carry out the factor separation analysis on a domain limited to the vicinity of Taiwan as shown in Fig. 22, which summarizes the rainfall for 13–18 June 2008 in the four experiments (Table 1). The calculations used to isolate the effects of the two factors and to show their

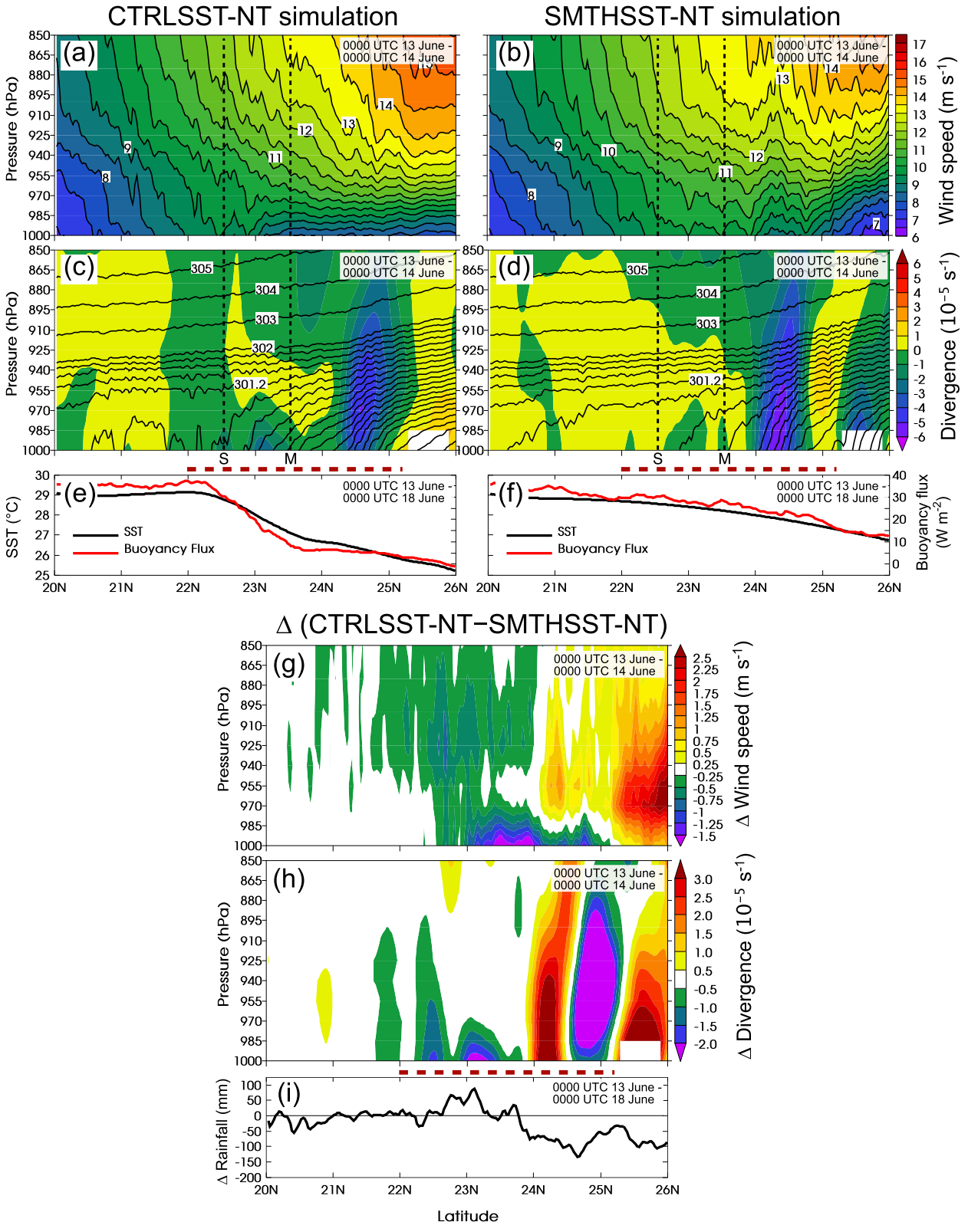

FIG. 19. As in Fig. 15, but for the NoTaiwan simulations with the island of Taiwan removed.

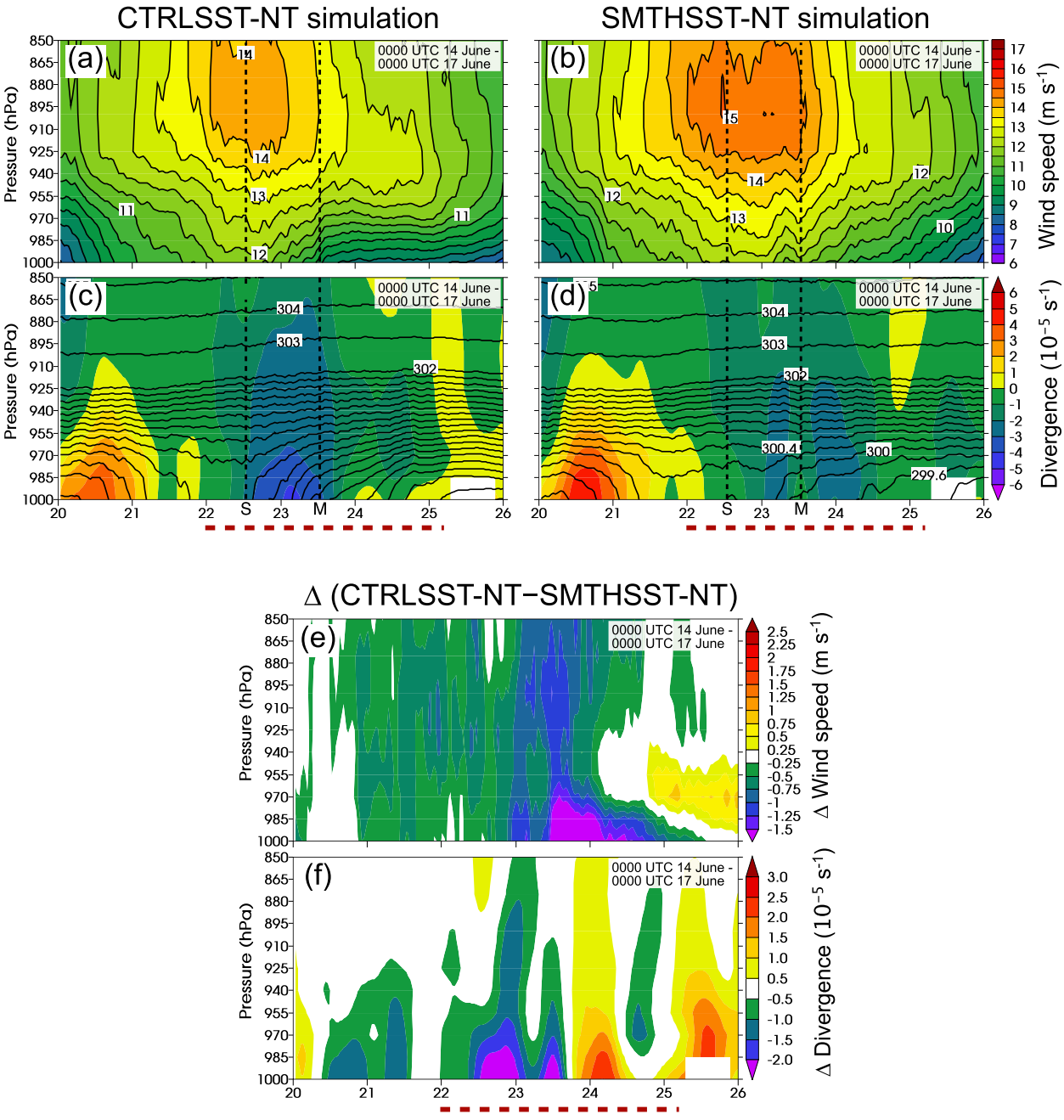

FIG. 20. (a)–(d) As in Figs. 19a–d and (e),(f) as in Figs. 19g,h, but time averaged over the period 0000 UTC 14 Jun–0000 UTC 17 Jun.

synergy is shown in Table 2. Note that the "base" component can be thought of as a starting point in which neither factor—SST front nor topography—is present. The sum of the four components equals the observed case: namely, the CTRLSST experiment (Fig. 22d). The synergy component is the difference between the difference plots shown in Fig. 23. Since these fields are similar, we expect the synergy to be small. Figure 24 shows the four components of the factor separation analysis. The largest contribution to the rainfall over the inland portion of southwestern Taiwan is from the "topography" component (Fig. 24b). Leeward of the Central Mountain Range a reduction of the rainfall owing to a rain shadow effect is evident. The "SST front" component (Fig. 24c) indicates the enhancement of precipitation owing to the front over the location of southwest Taiwan when the island is not present (a contribution of >125 mm). The "synergy" term (Fig. 24d) is small over southwestern

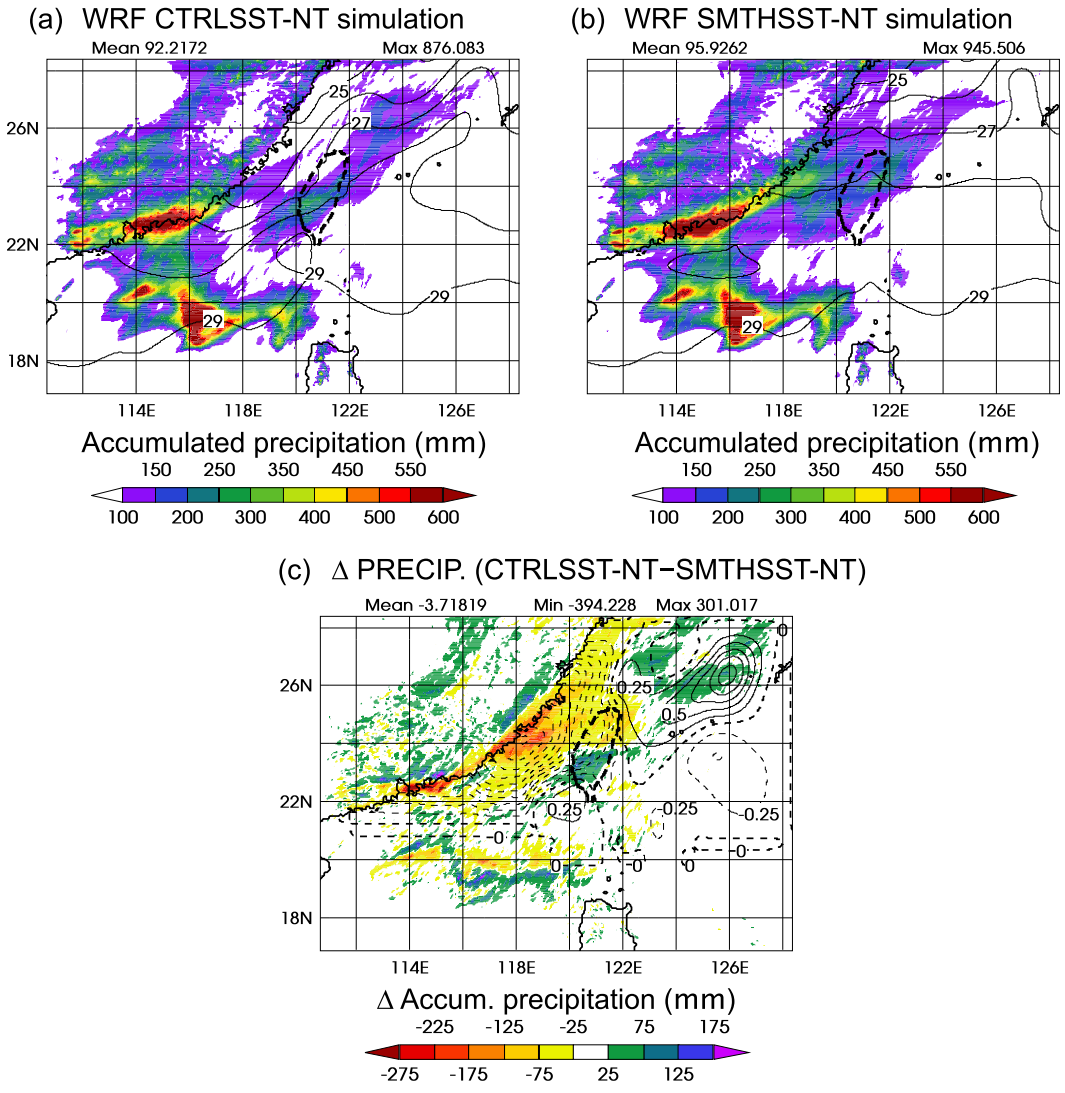

FIG. 21. Accumulated rainfall (color shading) from 0000 UTC 13 Jun through 0000 UTC 18 Jun from (a) CTRLSST-NT and (b) SMTHSST-NT simulations. SSTs (°C) are overlaid (contours). (c) Rainfall difference (color shading) between CTRLSST-NT and SMTHSST-NT simulations with SST difference overlaid (0.25°C contour interval with negative values indicated by dashed lines).

Taiwan, although there is generally a positive contribution to the rainfall along the southwest coastal area of about 75 mm because of a synergistic coupling between the SST front and the topography. This may be due to the eastward turning of the low-level flow toward the island owing to the SST front (see Fig. 16b), which would direct the flow more toward the CMR to enhance the mountain blocking effect. Over the northern part of the island the synergy term is rather large. The reason for this can be seen in Fig. 23. The SST difference has little effect on the rainfall in the northern part of the island (Fig. 23b) where the dominant effect on the airflow is the terrain. However, without the island present (Fig. 23a), the cooler waters to the north as a result of the SST front resulted in reduced rainfall amounts in the CTRLSST-NT simulation (Fig. 22c) versus the SMTHSST-NT simulation (Fig. 22a).

6. Summary and conclusions

WRF modeling experiments have been conducted to demonstrate the influence of a strong SST front off the southwest (upwind) coast of Taiwan on a heavy rainfall event during TiMREX on 13–18 June 2008. The SST front, which is a remnant of the East Asian winter monsoon, is typically present during the onset of the summer monsoon when the low-level flow switches from a northeasterly to southwesterly direction. We showed

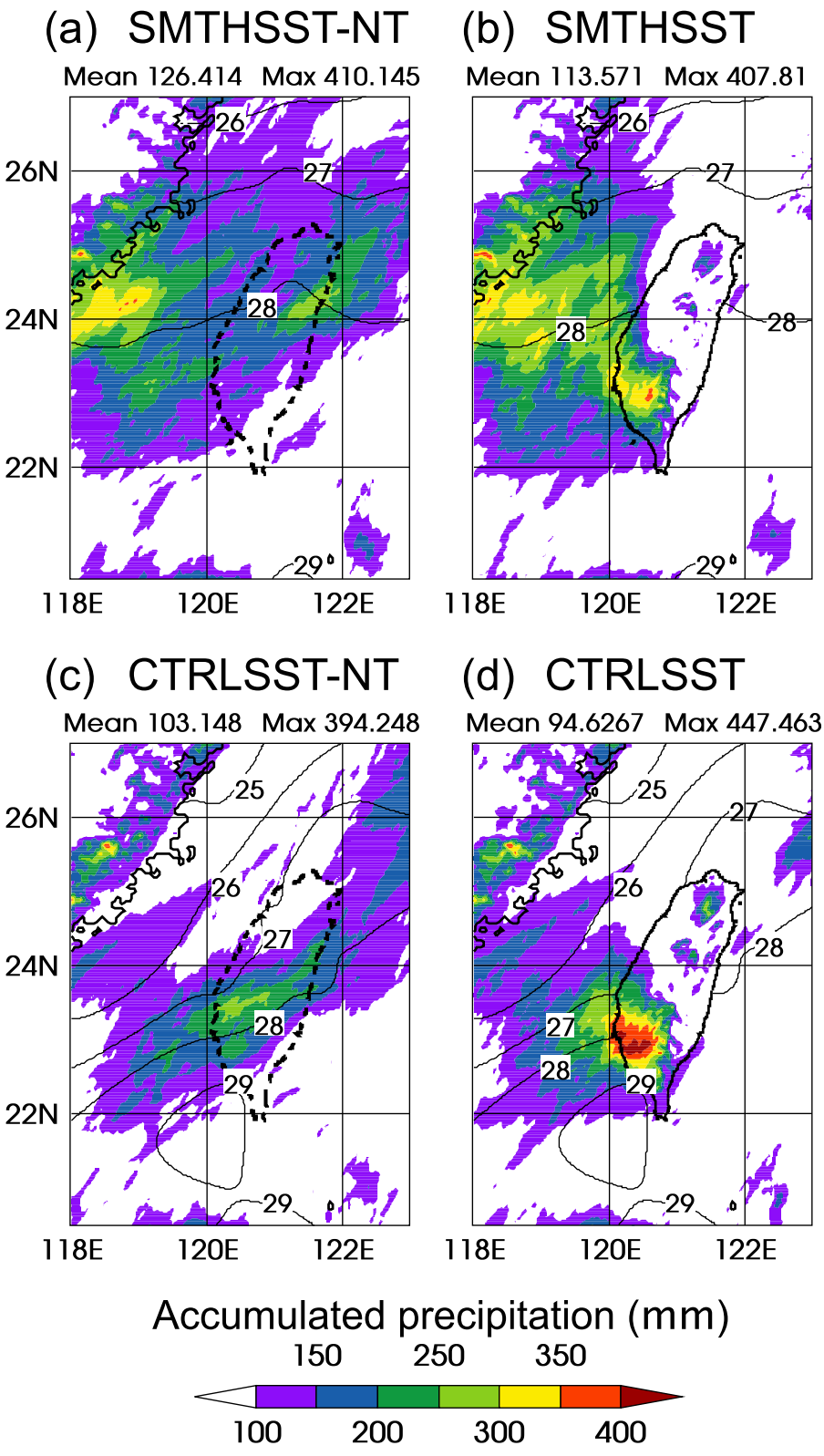

FIG. 22. Accumulated rainfall (mm, color shading) in the vicinity of Taiwan from 0000 UTC 13 Jun to 0000 UTC 18 Jun from (a) SMTHSST-NT, (b) SMTHSST, (c) CTRLSST-NT, and (d) CTRLSST simulations. SSTs (°C) are overlaid (contours).

TABLE 2. The four components of the factor separation analysis.

Factor	Name	Description	Calculation
f_0	Base	Part of the rainfall independent of the SST front and topography	f_0 = SMTHSST-NT
f_1	SST front	Sole contribution to the rainfall from the SST front	f_1 = CTRLSST-NT − SMTHSST-NT
f_2	Topography	Sole contribution to the rainfall from the topography	f_2 = SMTHSST − SMTHSST-NT
f_{12}	Synergy	Contribution to the rainfall from the synergistic effects of the SST front and topography	f_{12} = (CTRLSST − SMTHSST) − (CTRLSST-NT − SMTHSST-NT)

that, as the monsoon flow crossed the SST front, the PBL became stable over the colder waters to the north. Consistent with the vertical-mixing mechanism described by Wallace et al. (1989), there was a corresponding area of low-level convergence over the front that enhanced convective activity during the rainfall event. The results are also consistent with recent observational and modeling studies of the influence of SST fronts on convection (e.g., Minobe et al. 2008; Xu et al. 2011; Miyama et al. 2012).

We performed four experiments to assess the relative roles of the SST pattern and the orography of Taiwan. Two SST patterns were used to force the lower boundary—the observed SST with the strong gradient in the vicinity of Taiwan, and a smoothed SST field with a weak gradient. With each of these two fields, the model was run with the island of Taiwan in place and with the island replaced by ocean. For each of the four experiments, we performed seven ensemble runs with randomly perturbed initial conditions generated by the WRFDA

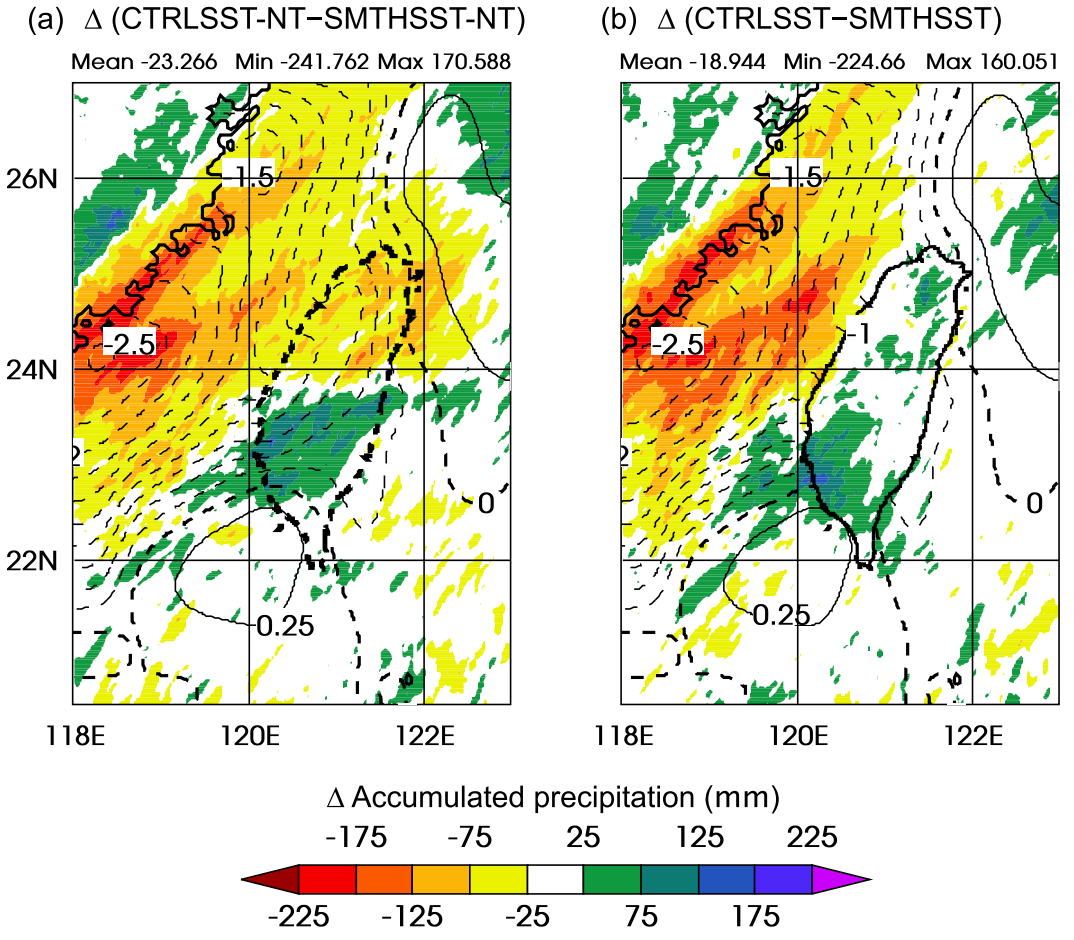

FIG. 23. Difference (CTRLSST − SMTHSST) in accumulated rainfall (mm, color shading) in the vicinity of Taiwan from 0000 UTC 13 Jun to 0000 UTC 18 Jun for (a) NoTaiwan simulations and (b) Taiwan simulations. The SST differences are overlaid (0.25°C contour interval with negative values indicated by dashed lines).

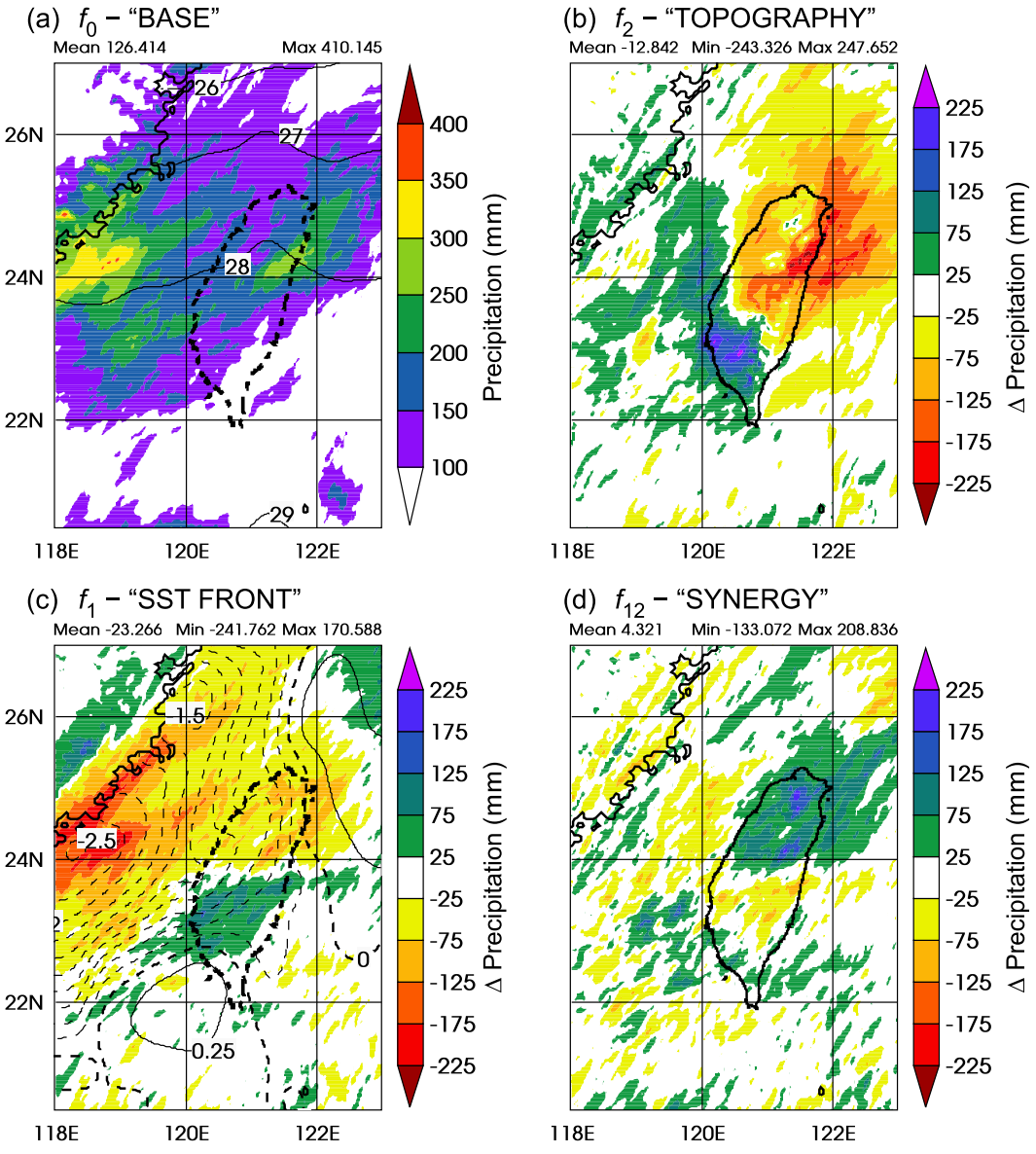

FIG. 24. The four factor separation components related to the accumulated rainfall in the vicinity of Taiwan from 0000 UTC 13 Jun to 0000 UTC 18 Jun—(a) the base (SMTHSST-NT) component with SMTHSST (°C) overlaid, (b) the topography component, (c) the SST front component with the SST difference overlaid (0.25°C contour interval with negative values indicated by dashed lines), and (d) the synergy component. (See Table 2.)

system. The results presented in the paper were the ensemble means of these runs. Both with and without the presence of island topography, the precipitation was considerably stronger over the location of southwest Taiwan when the strong SST gradient was present. While topographic effects explain most of the observed rainfall during the 13–18 June 2008 event, the presence of the SST front contributed about 65 mm to the peak rainfall amount over southwestern Taiwan when compared to the rainfall produced in simulations with the smoothed SST gradient. In terms of the areal averaged rainfall, the SST front resulted in an increase of about 21%.

The results of our study suggest that seasonal prediction of the potential severity of rainfall events associated with the East Asian summer monsoon over Taiwan may be improved by considering the SST pattern present at the monsoon onset. In some years, such as during the TiMREX field campaign of 2008, the SST front was anomalously strong and caused an enhancement of the rainfall by the southwesterly low-level jet that impinged on the island. In other years, the SST front

is not as strong and resembles the smoothed SST pattern used in our sensitivity study. In such years, the rainfall may not be as intense given a similar synoptic flow pattern as in 2008. An empirical study of past rainfall events and their correlation to SST patterns during the mei-yu season could support the applicability of our results of 2008 for other time periods and provide a valuable tool for seasonal prediction.

Acknowledgments. The authors thank Paul Ciesielski for providing the TiMREX radiosonde data and for general help with the TiMREX data. We also thank Dr. Christopher Davis of NCAR for providing the QPE SUMS data, Professor Russ Schumacher for help with implementing the WRFDA system in our experiments, and Professor Susan van den Heever for helpful advice on the factor separation analysis method. Three anonymous reviewers provided a number of suggestions that greatly improved the paper. We acknowledge high-performance computing support from Yellowstone (ark:/85065/d7wd3xhc) provided by the NCAR Computational and Information Systems Laboratory, sponsored by the National Science Foundation. This research was supported by National Science Foundation Grant AGS-0966758.

REFERENCES

Alpert, P., and T. Sholokhman, Eds., 2011: *Factor Separation in the Atmosphere: Applications and Future Prospects*. Cambridge University Press, 292 pp.

——, M. Tsidulko, and U. Stein, 1995: Can sensitivity studies yield absolute comparisons for the effects of several processes? *J. Atmos. Sci.,* **52,** 597–601, doi:10.1175/1520-0469(1995)052<0597:CSSYAC>2.0.CO;2.

Barker, D., W. Huang, Y.-R. Guo, A. J. Bourgeois, and Q. N. Xiao, 2004: A three-dimensional variational data assimilation system for MM5: Implementation and initial results. *Mon. Wea. Rev.,* **132,** 897–914, doi:10.1175/1520-0493(2004)132<0897:ATVDAS>2.0.CO;2.

——, and Coauthors, 2012: The Weather Research and Forecasting model's Community Variational/Ensemble Data Assimilation System: WRFDA. *Bull. Amer. Meteor. Soc.,* **93,** 831–843, doi:10.1175/BAMS-D-11-00167.1.

Bourras, D., G. Reverdin, H. Giordani, and G. Caniaux, 2004: Response of the atmospheric boundary layer to a mesoscale oceanic eddy in the northeast Atlantic. *J. Geophys. Res.,* **109,** D18114, doi:10.1029/2004JD004799.

Boyle, J. S., and T.-J. Chen, 1987: Synoptic aspects of the wintertime East Asian monsoon. *Monsoon Meteorology,* C.-P. Chang and T. N. Krishnamurti, Eds., Oxford University Press, 125–160.

Chelton, D. B., and S.-P. Xie, 2010: Coupled ocean–atmosphere interaction at oceanic mesoscales. *Oceanography,* **23,** 52–69, doi:10.5670/oceanog.2010.05.

Chen, C.-S., Y.-L. Chen, C.-L. Liu, P.-L. Lin, and W.-C. Chen, 2007: Statistics of heavy rainfall occurrences in Taiwan. *Wea. Forecasting,* **22,** 981–1002, doi:10.1175/WAF1033.1.

Chen, G. T.-J., 1983: Observational aspects of the Mei-Yu phenomenon in subtropical China. *J. Meteor. Soc. Japan,* **61,** 306–312.

——, 1992: Mesoscale features observed in the Taiwan Mei-Yu season. *J. Meteor. Soc. Japan,* **70,** 497–516.

Chen, J.-M., C.-P. Chang, and T. Li, 2003: Annual cycle of the South China Sea surface temperature using the NCEP/NCAR reanalysis. *J. Meteor. Soc. Japan,* **81,** 879–884, doi:10.2151/jmsj.81.879.

Chu, P. C., and C.-P. Chang, 1997: South China Sea warm pool in boreal spring. *Adv. Atmos. Sci.,* **14,** 195–206, doi:10.1007/s00376-997-0019-8.

——, S. Lu, and Y. Chen, 1997: Temporal and spatial variabilities of the South China Sea surface temperature anomaly. *J. Geophys. Res.,* **102,** 20 937–20 955, doi:10.1029/97JC00982.

Ciesielski, P. E., and R. H. Johnson, 2009: Atmospheric mixed layers over the South China Sea during SCSMEX. *SOLA,* **5,** 29–32, doi:10.2151/sola.2009-008.

——, and Coauthors, 2010: Quality-controlled upper-air sounding dataset for TiMREX/SoWMEX: Development and corrections. *J. Atmos. Oceanic Technol.,* **27,** 1802–1821, doi:10.1175/2010JTECHA1481.1.

Davis, C. A., and W.-C. Lee, 2012: Mesoscale analysis of heavy rainfall episodes from SoWMEX/TiMREX. *J. Atmos. Sci.,* **69,** 521–537, doi:10.1175/JAS-D-11-0120.1.

de Szoeke, S. P., and C. S. Bretherton, 2004: Quasi-Lagrangian large eddy simulations of cross-equatorial flow in the east Pacific atmospheric boundary layer. *J. Atmos. Sci.,* **61,** 1837–1858, doi:10.1175/1520-0469(2004)061<1837:QLESOC>2.0.CO;2.

Ding, Y., and J. C.-L. Chan, 2005: The East Asian summer monsoon: An overview. *Meteor. Atmos. Phys.,* **89,** 117–142, doi:10.1007/s00703-005-0125-z.

Dudhia, J., 1989: Numerical study of convection observed during the Winter Monsoon Experiment using a mesoscale two-dimensional model. *J. Atmos. Sci.,* **46,** 3077–3107, doi:10.1175/1520-0469(1989)046<3077:NSOCOD>2.0.CO;2.

Gourley, J. J., J. Zhang, R. A. Maddox, C. M. Calvert, and K. W. Howard, 2001: A real-time precipitation monitoring algorithm—Quantitative Precipitation Estimation and Segregation Using Multiple Sensors (QPE SUMS). Preprints, *Symp. on Precipitation Extremes: Prediction, Impacts, and Responses,* Albuquerque, NM, Amer. Meteor. Soc., 57–60. [Available online at https://ams.confex.com/ams/annual2001/techprogram/paper_18659.htm.]

Hayes, S. P., M. J. McPhaden, and J. M. Wallace, 1989: The influence of sea-surface temperature on surface wind in the eastern equatorial Pacific: Weekly to monthly variability. *J. Climate,* **2,** 1500–1506, doi:10.1175/1520-0442(1989)002<1500:TIOSST>2.0.CO;2.

Hong, S.-Y., and J.-O. J. Lim, 2006: The WRF Single-Moment 6-class Microphysics scheme (WSM6). *J. Korean Meteor. Soc.,* **42,** 129–151.

——, Y. Noh, and J. Dudhia, 2006: A new vertical diffusion package with an explicit treatment of entrainment processes. *Mon. Wea. Rev.,* **134,** 2318–2341, doi:10.1175/MWR3199.1.

Huffman, G. J., and Coauthors, 2007: The TRMM Multisatellite Precipitation Analysis (TMPA): Quasi-global, multiyear, combined-sensor precipitation estimates at fine scales. *J. Hydrometeor.,* **8,** 38–55, doi:10.1175/JHM560.1.

Johnson, R. H., and P. E. Ciesielski, 2002: Characteristics of the 1998 summer monsoon onset over the northern South China Sea. *J. Meteor. Soc. Japan,* **80,** 561–578, doi:10.2151/jmsj.80.561.

Jou, B. J.-D., W.-C. Lee, and R. H. Johnson, 2011: An overview of SoWMEX/TiMREX and its operation. *The Global Monsoon*

System: Research and Forecast, 2nd ed. C.-P. Chang et al., Eds., World Scientific, 303–318, doi:10.1142/9789814343411_0018.

Kuo, Y.-H., and G. T.-J. Chen, 1990: The Taiwan Area Mesoscale Experiment (TAMEX): An overview. *Bull. Amer. Meteor. Soc.,* **71,** 488–503, doi:10.1175/1520-0477(1990)071<0488:TTAMEA>2.0.CO;2.

Kuwano-Yoshida, A., S. Minobe, and S.-P. Xie, 2010: Precipitation response to the Gulf Stream in an atmospheric GCM. *J. Climate,* **23,** 3676–3698, doi:10.1175/2010JCLI3261.1.

Lai, H.-W., C. A. Davis, and B. J.-D. Jou, 2011: A subtropical oceanic mesoscale convective vortex observed during SoWMEX/TiMREX. *Mon. Wea. Rev.,* **139,** 2367–2385, doi:10.1175/2010MWR3411.1.

Li, J., and Y.-L. Chen, 1998: Barrier jets during TAMEX. *Mon. Wea. Rev.,* **126,** 959–971, doi:10.1175/1520-0493(1998)126<0959:BJDT>2.0.CO;2.

Li, Y., and R. E. Carbone, 2012: Excitation of rainfall over the tropical western Pacific. *J. Atmos. Sci.,* **69,** 2983–2994, doi:10.1175/JAS-D-11-0245.1.

Lin, Y.-L., 1993: Orographic effects on airflow and mesoscale weather systems over Taiwan. *Terr. Atmos. Oceanic Sci.,* **4,** 381–420.

Lindzen, R. S., and S. Nigam, 1987: On the role of sea surface temperature gradients in forcing low-level winds and convergence in the tropics. *J. Atmos. Sci.,* **44,** 2418–2436, doi:10.1175/1520-0469(1987)044<2418:OTROSS>2.0.CO;2.

Minobe, S., A. Kuwano-Yoshida, N. Komori, S.-P. Xie, and R. J. Small, 2008: Influence of the Gulf Stream on the troposphere. *Nature,* **452,** 206–209, doi:10.1038/nature06690.

Miyama, T., M. Nonaka, H. Nakamura, and A. Kuwano-Yoshida, 2012: A striking early-summer event of a convective rainband persistent along the warm Kuroshio in the East China Sea. *Tellus,* **64A,** 18 962, doi:10.3402/tellusa.v64i0.18962.

Mlawer, E. J., S. J. Taubman, P. D. Brown, M. J. Iacono, and S. A. Clough, 1997: Radiative transfer for inhomogeneous atmospheres: RRTM, a validated correlated-*k* model for the longwave. *J. Geophys. Res.,* **102,** 16 663–16 682, doi:10.1029/97JD00237.

O'Neill, L. W., S. K. Esbensen, N. Thum, R. M. Samelson, and D. Chelton, 2010: Dynamical analysis of the boundary layer and surface wind responses to mesoscale SST perturbations. *J. Climate,* **23,** 559–581, doi:10.1175/2009JCLI2662.1.

Ruppert, J. H., Jr., R. H. Johnson, and A. K. Rowe, 2013: Diurnal circulations and rainfall in Taiwan during SoWMEX/TiMREX (2008). *Mon. Wea. Rev.,* **141,** 3851–3872, doi:10.1175/MWR-D-12-00301.1.

Sasaki, Y. N., S. Minobe, T. Asai, and M. Inatsu, 2012: Influence of the Kuroshio in the East China Sea on the early summer (baiu) rain. *J. Climate,* **25,** 6627–6645, doi:10.1175/JCLI-D-11-00727.1.

Seigel, R. B., S. C. van den Heever, and S. M. Saleeby, 2013: Mineral dust indirect effects and cloud radiative feedbacks of a simulated idealized nocturnal squall line. *Atmos. Chem. Phys.,* **13,** 4467–4485, doi:10.5194/acp-13-4467-2013.

Skamarock, W. C., and J. B. Klemp, 2008: A time-split nonhydrostatic atmospheric model for weather research and forecasting applications. *J. Comput. Phys.,* **227,** 3465–3485, doi:10.1016/j.jcp.2007.01.037.

——, and Coauthors, 2008: A description of the Advanced Research WRF version 3. NCAR Tech. Note TN-475+STR, 125 pp.

Skyllingstad, E. D., D. Vickers, L. Mahrt, and R. Samelson, 2007: Effects of mesoscale sea-surface temperature fronts on the marine atmospheric boundary layer. *Bound.-Layer Meteor.,* **123,** 219–237, doi:10.1007/s10546-006-9127-8.

Small, R. J., and Coauthors, 2008: Air–sea interaction over ocean fronts and eddies. *Dyn. Atmos. Oceans,* **45,** 274–319, doi:10.1016/j.dynatmoce.2008.01.001.

Stein, U., and P. Alpert, 1993: Factor separation in numerical simulations. *J. Atmos. Sci.,* **50,** 2107–2115, doi:10.1175/1520-0469(1993)050<2107:FSINS>2.0.CO;2.

Stull, R. B., 1988: *An Introduction to Boundary Layer Meteorology*. Kluwer Academic, 666 pp.

Tanimoto, Y., T. Kanenari, H. Tokinaga, and S.-P. Xie, 2011: Sea level pressure minimum along the Kuroshio and its extension. *J. Climate,* **24,** 4419–4434, doi:10.1175/2011JCLI4062.1.

Thiébaux, J., E. Rogers, W. Wang, and B. Katz, 2003: A new high-resolution blended real-time global sea surface temperature analysis. *Bull. Amer. Meteor. Soc.,* **84,** 645–656, doi:10.1175/BAMS-84-5-645.

Varikoden, H., A. A. Samah, and C. A. Babu, 2010: The cold tongue in the South China Sea during boreal winter and its interaction with the atmosphere. *Adv. Atmos. Sci.,* **27,** 265–273, doi:10.1007/s00376-009-8141-4.

Wallace, J. M., T. P. Mitchell, and C. Deser, 1989: The influence of sea-surface temperature on surface wind in the eastern equatorial Pacific: Seasonal and interannual variability. *J. Climate,* **2,** 1492–1499, doi:10.1175/1520-0442(1989)002<1492:TIOSST>2.0.CO;2.

Wang, C.-C., and G. T.-J. Chen, 2003: On the formation of leeside mesolows under different Froude number flow regime in TAMEX. *J. Meteor. Soc. Japan,* **81,** 339–365, doi:10.2151/jmsj.81.339.

——, ——, T.-C. Chen, and K. Tsuboki, 2005: A numerical study on the effects of Taiwan topography on a convective line during the mei-yu season. *Mon. Wea. Rev.,* **133,** 3217–3242, doi:10.1175/MWR3028.1.

Xie, S.-P., H. Xu, N. H. Saji, Y. Wang, and W. T. Liu, 2006: Role of narrow mountains in large-scale organization of Asian monsoon convection. *J. Climate,* **19,** 3420–3429, doi:10.1175/JCLI3777.1.

Xu, H., M. Xu, S.-P. Xie, and Y. Wang, 2011: Deep atmospheric response to the spring Kuroshio over the East China Sea. *J. Climate,* **24,** 4959–4972, doi:10.1175/JCLI-D-10-05034.1.

Xu, W., E. J. Zipser, and C. Liu, 2009: Rainfall characteristics and convective properties of mei-yu precipitation systems over South China, Taiwan, and the South China Sea. Part I: TRMM observations. *Mon. Wea. Rev.,* **137,** 4261–4275, doi:10.1175/2009MWR2982.1.

——, ——, Y.-L. Chen, C. Liu, Y.-C. Liou, W.-C. Lee, and B. J.-D. Jou, 2012: An orography-associated extreme rainfall event during TiMREX: Initiation, storm evolution, and maintenance. *Mon. Wea. Rev.,* **140,** 2555–2574, doi:10.1175/MWR-D-11-00208.1.

Yeh, H.-C., and Y.-L. Chen, 2002: The role of offshore convergence on coastal rainfall during TAMEX IOP 3. *Mon. Wea. Rev.,* **130,** 2709–2730, doi:10.1175/1520-0493(2002)130<2709:TROOCO>2.0.CO;2.

Yu, C.-K., B. J.-D. Jou, and D. P. Jorgensen, 2001: Retrieved thermodynamic structure of a subtropical, orographically influenced, quasi-stationary convective line. *Mon. Wea. Rev.,* **129,** 1099–1116, doi:10.1175/1520-0493(2001)129<1099:RTSOAS>2.0.CO;2.